CHARACTERISING THE OPTICAL VARIABILITY OF WOLF-RAYET STARS USING TESS OBSERVATIONS

by

KHANG M. NGUYEN

&

SUPERVISED BY: DR. IAN STEVENS

School of Physics and Astronomy

College of Engineering and Physical Sciences

University of Birmingham

Monday 16th May, 2022

Abstract

Wolf-Rayet stars (WRs) are hot and massive stars with masses ranging from about 10 to 25 solar masses, coupled with their very high mass loss rate through their stellar winds. These dense stellar winds are radiatively-driven, their driving mechanism relies on momentum transfers of photons, via repeated absorptions or scatterings of multiple spectral lines, to their winds. However, this driving is heavily dependent on the velocity gradient of the stellar winds, which are supersonic by nature. Thus, this leads to the winds being intrinsically very unstable, leading to instabilities arising within the winds, which have observational consequences at a range of wavelengths.

Given the rise of space-borne observational powers (such as TESS), it is now possible to study the optical variability of Wolf-Rayet stars to high precision. In addition to variability associated with the complex wind behaviour, these stars also show variability due to stellar eclipses, wind eclipses, and pulsations (often from a companion star).

In this project, I am looking at the 2-min cadence data of a sample of 58 bright Wolf-Rayet stars observed by the NASA TESS satellite. The goals of this project are to characterise the optical variability of these Wolf-Rayet stars and to better constrain their nature via thorough time-series analysis.

Acknowledgements

I would like to sincerely and emphatically thank my supervisor, Dr. Ian Stevens for your immense support of my efforts in your project and also your support as a mentor for guiding me in my endeavours of applying for post-graduate studies.

I would also like to thank all of my friends, family and loved ones for sticking by me and offering your undying support to my passion and my journey thus far.

Contents

Chapter 1

Introduction

Classic Wolf-Rayet (WR) stars are essentially evolved, young and massive stars that have shed their outer hydrogen layers and is in the process of fusing helium and heavier metals within their core. As such, they are some of the hottest and most luminous objects in the stellar population with a stellar luminosity ranging from the hundred-thousands to millions of times the solar luminosity (Crowther, 2007). They are the finale of the evolution of massive O stars, boasting with masses typically ranging anywhere between 10-25 $M_{\odot}$ to even beyond that.

In terms of spectroscopy, WRs possess strong and broad emission lines atypical of the usual narrow-band absorption lines shown by your average star. In a population of Wolf-Rayet stars however, it soon became clear that there was a split between two different types of dominant spectra that was observed. The first type, called WN subtypes, are those that show strong emission lines of helium and nitrogen in their spectra. With the second type being the WC and WO subtypes, in which they had prominent lines of helium, carbon (C) and oxygen (O). These subtypes are eventually divided up into many levels within the same subtype, as these levels follow from whichever dominant ionised line is observed.

For example, in the WN sub-class, the levels go from WN2 with the requirement that there is no N_V and N_{IV}, to WN11 where $N_{III} \approx He_{II}$ or that N_{III} is either weak or absent. These WN criteria are set by Smith et al. (1996). Other sub-classes would have their own criteria to

follow as well, namely both WC and WO sub-classes have to obey quantitative criteria laid out by Crowther et al. (1998).

There also exist an entire 'sub-species' of stars that show intermediate spectral features, crossing back and forth around what would be an O-star and what would be a WR-star. These stellar sub-species are called slash stars (Crowther and Walborn, 2011). Their associated slash notation of the spectral types take a form like this O3If*/WN6, and it was first used by Walborn (1982).

Wolf-Rayet stars plays an impactful role within their local interstellar medium theatre. As they are extremely hot, they provide feedback of ionising photons to their surroundings (Sander et al., 2012; Hamann et al., 2006). Additionally, they also spew their guts out (stellar mass loss) to their environments, incidentally enriching the ISM with metals and influencing the chemical compositions around their vicinity (hence influencing star formations around these areas as well). These lost material are carried outward by their extremely fast and dense stellar winds. These supersonic winds are inherently unstable by nature due to them being radiatively-driven by absorptions and scatterings of many spectral lines. And with the presence of instabilities in their winds, one can observe its effects upon the star's optical variability itself. Luckily, these phenomena are becoming increasingly accessible for research via the advanced development of space-borne observatories, the capabilities of asteroseismology. These factors have allowed interests in Wolf-Rayet stellar wind structures to flourish and hence come an increasing number of research projects surrounding this topic.

In this report, I present my attempt at characterising the optical variability of a wide selection of Wolf-Rayet stars using 2-minute cadence data obtained from the NASA Transiting Exoplanet Survey Satellite (TESS). The layout of content will be as follows: Chapter 2 will describe the data selection process and subsequent analysis methods used in this study. Chapter 3 will present a select number of results sorted by its spectral types, chosen due to its interesting outcomes and will be followed by a discussion in Chapter 4 of the implications and future prospects that these results could potentially yield. Finally, this report is rounded off by a conclusion in Chapter 5. Be duly noted that this report does not cover every individual stars in my sample, one may find, however, the full result dataset linked in the Appendix B.

Chapter 2

Data and Methods

The data used in this study was first based of using the online Galactic Wolf Rayet Catalogue that was compiled by Rosslowe and Crowther (2015). This catalogue contains a known total of 760 galactic WR stars at our disposal. The next step is to then filter out a handful of the brightest WRs to work with, we applied a criteria that these stars must have a magnitude of $V < 12$ in order to be selected. This eventually shortlisted the catalogue to about 90 WRs left.

From this narrowed-down list, I proceeded to check each star for their TESS time series data availability. The Transiting Exoplanet Survey Satellite (TESS) is a satellite built by NASA that was launched in 2017. TESS is tasked to observe each designated star for an interval ranging from a month to a year, in which the duration depends on the star's ecliptic latitude which depending mainly on the star's ecliptic latitude. The satellite observatory takes brightness measurements of its target stars in 2-minute cadences, and full frame images (FFIs) in 30-min cadences (Ricker et al., 2014).

Specifically, I am searching for any 2-minute cadence data that TESS had captured of our WR candidates to use for this study. This is done by utilising the Web TESS Viewing Tool (WTV) to look at sectors that these stars found themselves in and was observed by the TESS satellite. I then downloaded any available 2-minute cadence data via the MAST archive using a search radius of about 40 arcsec. This radius should ensure that I only find the exact WR target I needed, and

if anything else appear on my search that has a radius value larger than the primary result, would be excluded from the search as it is likely an irrelevant target. This further brought down the amount of targets in my sample to a total number of 59 WR stars left. Though, several targets would have multiple light curves (per star) available and hence the total amount of light curves that was obtained in the end was almost 100 in total.

I am mainly working off from the Python library *lightkurve* by Lightkurve Collaboration et al. (2018) to treat our innumerous amount of time-series data.

After obtaining the time-series data from TESS, specifically the PDCSAP (Pre-search Data Conditioning Simple Aperture Photometry) flux as it is more carefully cleaned and treated than the SAP version, I find the period-at-max-power of each star's light curve data (via *lightkurve*) and then proceeded to fold their light curves onto each other using only this maximum period at first. Then, I would fold them again, but separate from the previous fold, by multiplying their period-at-max-power by 4 and applying a wrapping phase of 0.2. This procedure would create two folded light curve plots for each light curve of each WRs, as shown in ample amounts in Appendix. A. This procedure is done to pre-inspect a star's periodicity and whether it is obvious from first glance or not and what the time-series data imply about the star's behaviour.

I then generate Lomb-Scargle periodograms of each star in order to also inspect if there is any obvious periodicity and inspecting the entire curve's shape profile. Then, using the Bayesian MCMC framework via the Python code *emcee* (Foreman-Mackey et al., 2013), I initially fit these Lomb-Scargle periodograms using the amplitude spectrum function defined by Bowman et al. (2019) as written below:

$$\alpha(\nu) = \frac{\alpha_0}{1 + (\frac{\nu}{\nu_{\text{char}}})^{\gamma}} + C_w$$

where α_0 represents zero-frequency amplitude, γ is the logarithmic amplitude gradient, ν_{char} is the characteristic frequency which varies inversely to the characteristic timescale such that $\nu_{\text{char}} = (2\pi\tau)^{-1}$, and C_w is a frequency-independent white noise term (Blomme et al., 2011).

However, my curiosity ventures further as I decided to test with modifying the initial equation above by supplying an additional Cauchy distribution term, in order to identify peak positions that are present within my sample of periodograms. The modified equation goes as such:

$$\alpha(\nu) = \frac{\alpha_0}{1 + (\frac{\nu}{\nu_c})^\gamma} + C_w + \frac{1}{\pi\lambda}\left[\frac{\lambda^2}{(\nu - \nu_0)^2 + \lambda^2}\right] \tag{2.1}$$

where ν_0 specifies the location of the peak and λ is the scale parameter dictating the half-width-half-maximum (HWHM) and the rest of the parameters are the usuals as specified by Bowman et al. (2019)

Following this routine, I then was able to generate and calculate the fits of all my Wolf-Rayet stars that are in my chosen sample. The results are further discussed in the next section with all subsequent plots of any mentioned Wolf-Rayet stars, are moved towards Appendix A to preserve the reader's flow.

Chapter 3

Results

In this section I will be evaluating a portion of results from the entire sample that stood out in terms of their fitted power spectrum and their observable physical properties. In order to preserve the pacing of this section, I will put all relevant figures in Appendix A. The reader may also find the public repository containing all the obtained results from my 58 Wolf-Rayet stars sample in Appendix B. Finally, Table C contains all the numerical MCMC fit parameters of the amplitude spectrum of the entire Wolf-Rayet sample.

3.1 Single WN Stars

WR6

WR 6 is a star with the sub-class of WN4b and is one of the brightest and well-known Wolf-Rayet stars discovered to date. It is also known to be a binary carrying a single O-star. However, according to Oskinova (2005), its companion O-star contribution towards the system's overall flux is minimal (X-ray flux measured to be too low for a high-mass X-ray binary) and hence we can consider this system to be a 'single' star. Its apparent magnitude varies with a period of roughly 3.7 days (St-Louis et al., 1995) though it fluctuates and is not stable, even at times not even

showing any signs of variability. This is shown via the Lomb-Scargle periodograms of its TESS light curves in Figure. A.2, as only one out of three datasets return a period-at-max-power of about 3.7 days whilst the others are roughly 1.8 days. (Morel et al., 1997) argued that WR 6's unstable period measurements are due to effects of rotations of structured wind called *Corotating Interaction Regions* (**CIRs**), and not due to its binarity status.

Interestingly, its light curve shown in Figure. A.1, shows a rather clean pattern where its folded fluxes overlap each other quite nicely, suggesting a clear period to be distinguished. But its fitting results highly contrast its otherwise 'tame' first look. All three of its amplitude spectrum fits struggle to model its signals (Figure. A.2), with the first dataset returning an absurdly high γ value for its logarithmic gradient and all of them fail to estimate the region of white noise. One of the fits did manage to detect the highest peak of the periodogram however, they still struggle overall in fitting WR 6's variability.

WR12

According to Rauw et al. (1996), WR 12 is supposed to be a binary system classed as a WN8h+? and with a period of 23.9 days. Hamann et al. (2019) affirms that it is a binary system with colliding winds, but still finds no indications of any accompanying OB-type star and thus it is still considered as a single-star system.

Its light curve in Figure A.3 does not show any obvious periodicity in the 2-minute cadence data and hence the phase folded light curve also does not tell us much about its system. This resulted in its periodogram (Figure A.4) taking more of a uniform (and logarithmic) downward slope towards the higher frequencies. Since its period is quite long compared to the (low) resolution of the lower frequencies of the power spectrum, the amplitude spectrum fit simply could not find its true frequency despite fitting the signal quite well.

WR40

WR 40 is a WN8h class star that innately shows a large variability within every spectral bands. The erratic patterns of this star's variability was found to have an underlying coherence pattern by Matthews and Moffat (1994). They discovered that the wide range of WR 40's periods (2-7 days) are actually just harmonics of two longer periods, that of 12.3 and 17.5 days. Indeed, they also attempt to recreate this behaviour by simulating an eclipsing binary with one asynchronously-rotating component, implying that WR 40 should be a binary system. However, this was argued against as there were no detections (or rather faint) of X-ray emissions from the system (Oskinova, 2005).

One can inspect this chaotic behaviour in Figure. A.5, especially in its phase-folded light curve. Across all three datasets available for WR 40, each one yielded a different period-at-max-power and when folded onto each other, all produced a different and unpredictable time series. This does reflect somewhat onto the amplitude spectrum fits in Figure. A.6. As in the third set of light curve, the fit was finding a hard time converging to a conclusive solution, whereas the first two sets both have tighter spreads of solutions with none of them having extremely steep log-gradients when modelling the signal.

WR66

WR 66 was classified as a WN8(h) with a compact companion, with previous studies suggesting WR 66's companion is spiraling inwards to it. But this idea was argued against by Rauw et al. (1996) favouring another mechanism (non-radial pulsation) that was more prominent amongst the wider WN8-subtype species. What is more interesting about this star can be seen in the fitted periodograms of both datasets in Figure. A.8, where both of them showed a significant increase in amplitude power towards the higher frequency range (≈ 7 day^{-1}). The fitted model also detected the highest peak of both sets at 6.93 day^{-1} despite both determining $\nu_{\rm char} \approx 2$ day^{-1}. This signature is rather unique in that it suggests WR 66 has a very fast orbital period, which are uncommon within the scope of my sample, or it does suggest other mechanisms are at play. For

example, WR 66's fainter visual companion might have interfered with the astrometry (Hamann et al., 2019) or the fact that WR 66 might be affected by other members of its association Anon Cir OB1 (Lundstrom and Stenholm, 1984).

3.2 Single WC Stars

WR23

WR 23 is a WC6 belonging to the Carina OB1 association (van der Hucht, 2001; Sander et al., 2012). The light curves obtained from this star is an example of its signals being dominated by noise, hence making the job of distinguishing its period much tougher. One may still be able to peer into the phase-folded + wrapped light curve in Figure. A.9 and could still detect a weak undulation of its flux. Even so, this does not translate well to fitting its periodogram in Figure. A.10. Despite the fit following closely along WR 23's power spectrum, one can observe that it clearly struggles in determining which is the definite peak of the periodograms. Which is evident that more treatment and cleaning of the data is needed for stars such as those of WR 23, before processing it even further.

WR59

WR 59 belongs to the sub-class of WC9d and is also speculated to be a binary system due to the detection of Balmer absorption features made by Williams et al. (2005).

It only possesses one set of measurement and upon folding it in Figure A.11, yields a very disjointed light curve that does not convey much useful information. However, its periodogram in Figure A.12 does not resemble most of the stars that we have already seen, except only for the second periodogram of WR 12 in terms of its logarithmically descending power and enormous α_0 value. Thus, similarly to WR 12, its amplitude spectrum fit could not determine any certain

periodicity that may exist and would warrant data with longer cadences in hopes of uncovering more information behind these specific types of stars.

3.3 Slash Stars

WR43 A, B, C

WR 43 is a peculiar target due to the fact that it is observed to be the core of a young, massive and unevolved Galactic cluster called NGC 3603 (Schnurr et al., 2008). The Wolf-Rayet core consists of three WN6ha stellar components that are subsequently named as WR 43A, 43B and 43C. 43A is a known double eclipsing binary with a 3.77 days orbital period (Moffat and Niemela, 1984), whilst 43C is a newly discovered binary made by Schnurr et al. (2008), and 43B was concluded to be a lonesome WN6ha star in this Wolf-Rayet triad.

WR 43A would get the most attention here as Schnurr et al. (2008) managed to derive the separate binary component's masses and confirm that they are identical in terms of spectral types (both WN6ha). Meanwhile, according to the Rosslowe and Crowther (2015) catalogue, WR 43C is of spectral type O3If*/WN6 which meant that the visible component in the WR 43C binary is a slash star, and not a WN6ha star as thought by the former study.

However, given this fact still, the TESS observations of this system consisted of only one light curve that is duplicated across all of its three components. Hence, in Figure. A.15 and Figure. A.16, one may see that because the light curve is identical across the board, the amplitude spectrum fit would also be (roughly) identical as well. The only parameter with some discernable difference is the value of α_0 throughout each components, otherwise every other parameters are mostly the same. The peak location from the fit is exactly half the actual period of WR 43A, but this is only due to the system's eclipsing binarity. A secondary peak is observed at around 1 day^{-1} and I suspect that this might be contributions from either one of 43B and/or 43C.

WR25

WR 25 is my sample's first and only instance of a slash star binary, specifically classed as O2.5If*/WN6+O. According to Hamann et al. (2019), WR 25 has a X-ray light curve which determined its period to be 208 days and is also a WR+O colliding wind system (Pandey et al., 2014; Pradhan et al., 2021). Gamen et al. (2008) had also calculated the system's eccentric orbit and claimed that the its components would have minimum masses of $75 + 27M_{\odot}$.

With this in mind, one may expect that the light curves present for WR 25 to be complex at the very least. This is true as Figure. A.13 illustrates. Its folded light curves are reminiscent to that of WR 40's chaotic behaviours, and this would remain true to all of its available light curves as well. However, in contrast to WR 40, the amplitude spectrum MCMC fits turned out to do a good job in fitting all three of WR 25's power spectrum (Figure. A.14), even identifying a consistent peak around the 1 day^{-1} mark across all datasets.

3.4 Wolf-Rayet Binaries (WRBs)

WR46

This is a rather controversial star in that there are many arguments regarding its true nature and binarity. WR 46 is currently classed as a WN3p+OB? according to van der Hucht (2001) catalogue. Comments from Hamann et al. (2006) about previous studies of this star, where he cited one that found its radial velocity period to be at 0.329 days and proposed that its binary companion is a neutron star with an accretion disk. Another cited study found that its photometric period to be 7.46 days, and yet they cited another different study that argued for this system to be a non-radial pulsator instead of a binary system. Hamann et al. (2006) eventually treated this system as a single-star system until its binarity is more concretely confirmed.

Similarly, its TESS observations have also revealed some intriguing results in both its light

curves in Figure. A.17 and amplitude spectrum fit in Figure. A.18. It is obvious by inspection that the simple model that is used in this study is insufficient in fully describing what is happening in WR 46's periodograms. In which its profile noted the presence of two 'mountains' of near identical powers towards the frequency range of 1-10 day^{-1}, and a large peak (albeit less resolved) prior to that as well. The semi-Lorentzian fit definitely struggled to model this star's power spectrum, and hence could not provide reliable fit parameters that could at least give us some useful hints towards the nature of WR 46.

WR86

WR 86 is a WC7 star with a B0III companion that is already known as a visual binary. Its variability was initially measured by Monderen et al. (1988) to be around 3 hours and then contributions of a possible β-Cephei companion would soon be considered by van Genderen et al. (1991). Latter variability studies made by Paardekooper et al. (2002) would update upon these values, revealing two photometric periods of near-equal amplitudes (3.504 & 3.264 hours). Though, the author did conclude that the photometric behaviours are mostly from of the β-Cephei companion rather than the Wolf-Rayet star.

Thus at first glance of the periodogram of WR86 in Figure. A.20, one may think that WR 86 has an unusually high orbital frequency compared to the stars that we had already considered prior. The fit is, nonetheless, accurate in modelling the signal and detecting the correct maximum peak and returning a variability of roughly 3 hours also, matching those of Paardekooper et al. (2002). What it does not tell us is that it is largely the work of the binary's β-Cephei companion.

WR31

WR 31 is of spectral type WN4o+O8V with a known period of around 4.83 days (Fahed and Moffat, 2012). In this instance, the star's folded light curves (Figure. A.21) showed signs of a discernable periodicity underneath what looks like just a smear of noisy data on top. In its

periodogram fit (Figure. A.22), the amplitude function fails to locate the peak that was meant to be its true period according to Fahed and Moffat (2012) but did a good job in tracing out the entirety of the signal regardless. What is interesting are the 'pulses' that the periodogram exhibits towards the higher frequency end. These numerous peaks are what is getting picked up by the fitting model, and they all rose at equally-spaced frequency from each other for about four times before it subsided to the white-noise region of the signal.

WR139

Upon analysing the results of WR 139, one can see its similarities to WR 31 in terms of its behaviour in its periodograms (equally-spaced 'pulses'). Except, WR 139 possesses three light curves to be inspected and it is an eclipsing binary whereas WR 31 is not. WR 139 is a WN5o+O6III-V binary with a known period of roughly 4.2 days (Rosslowe and Crowther, 2015). It is also the brightest disc-eclipsing WR+O binary amongst its kind, which makes it of huge importance for the studies of colliding winds (Stevens and Howarth, 1999).

If one inspects its folded light curves in Figure. A.23, it's clear that they overlap quite nicely however, there are two depths present in this overlap, suggesting strongly that one of those depths is the period belonging to its O6III-V companion. In all of its periodograms in Figure. A.24, they all displayed that same 'pulsing' behaviour such as those of WR 31, if anything the pulses are even sharper. I speculate its cause has to be somewhat involved with the phenomena of colliding winds, since both WR 139 and WR 31 are studied targets for this phenomena in Fahed and Moffat (2012) and Stevens and Howarth (1999).

Chapter 4

Discussions

As we can see from the selection of results obtained above, each Wolf-Rayet stars' behaviours are unique with most of them possessing at least a notable feature distinct from one another. However, this step of utilising the MCMC algorithm to fit a semi-Lorentzian profile onto each star's periodogram is only the beginning of laying down the foundations for further (and more complex) analysis in the future. In this section, I will briefly discuss first about my altered version of Bowman et al. (2019)'s amplitude spectrum function and its usage within this project. Then I will move onto briefly describe the steps and potential directions that is present ahead of this project's current outcomes.

With my modified amplitude spectrum function, it provided an unforeseen opportunity for the MCMC fit to pinpoint sharp peaks that the unaltered function would have missed. As observed from Table. C, the characteristic frequency, ν_{char}, would often not correspond to the light curve's peak and in many cases would return a number that is either buried deep in (high-frequency range) noise or located where there is almost no data (low-frequency range). The Cauchy distribution term offered the extra help in characterising the system's orbital frequency and at many times, re-confirming known periods from literature.

One potential downside to this modified model is its troubles with producing corner plots of the posteriors after the fit. This report does not incorporate any posterior plots resulting from

this modified model into the main analysis yet. The main issue at hand is due to a limitation in computing power, I had to reduce the number of walkers and iterations in my MCMC algorithm to achieve a balance between a good fit in the best-possible time. This created a dilemma in which the posteriors did not have enough data points to create contours for the corner plots. This created a follow-up issue, demonstrated in Figure. 4.1 below, in which the corner plot showed very scattered concentrations of the best-fit parameters. What might be of interest is the faint traces that they left behind along the path to the concentrated clusters and what they mean. However, it does not change the fact that this combined model's posterior corner plot is erroneous and will not be included (yet) in my analysis.

A common procedure that is observed in Bowman et al. (2019) and Lenoir-Craig et al. (2022) is called 'pre-whitening'. This procedure involves evaluating the signal-to-noise ratio (SNR) amplitude of each peak that is seen in the star's Lomb-Scargle periodogram and removes any shown periodicities out from the observations prior to analysis, and subsequent MCMC fittings of the amplitude spectrum. This technique is done with the purpose of studying the low-frequency stochastic variability that is present within these Wolf-Rayet stars.

In actuality, the initial objective of this project was to probe and enter the territories of the study of chaos and whether it can be detected and characterised from within Wolf-Rayet stars' unstable stellar winds. And hence, pre-whitening the signal would have been an essential step in order for this to happen. Post-whitening best-fit parameters would serve as the basis for introducing analysis techniques from non-linear dynamics. Phillipson et al. (2018, 2020) had approached Wolf-Rayet stars in this regard and delve into analysing complicated dynamical WR systems in their studies. Another exciting aspect that awaits exploration is the idea of creating chaos decision trees with a structure similar to that of Toker et al. (2019) but for astrophysical purposes. This decision tree would help in the detection of chaos in noisy signals which can be useful for quite a lot of WRs in my sample whose signals are very noise-dominated.

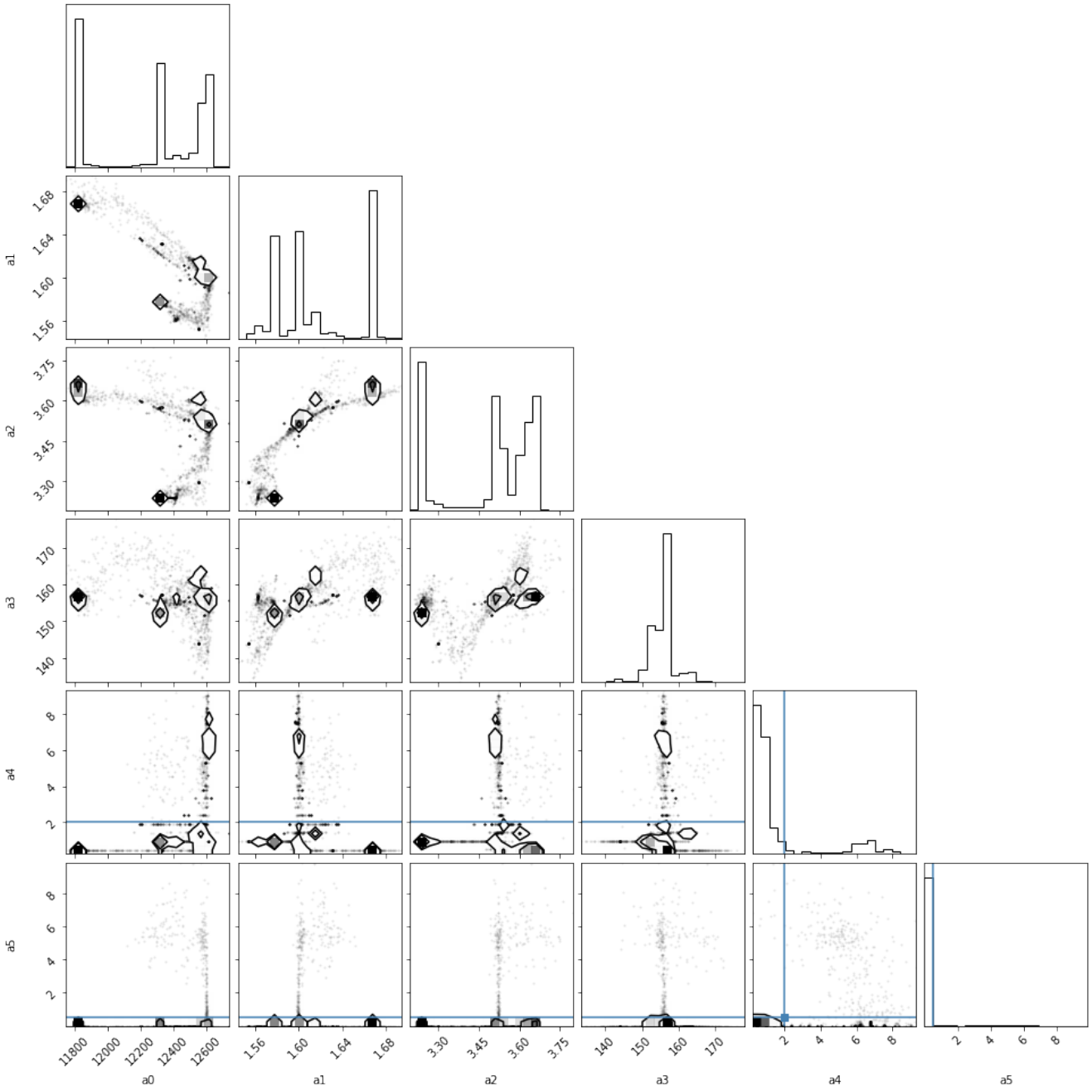

Figure 4.1: Erroneous posterior corner plot of WR 139 fit parameters

The avenues in which the results of this project could aid in is also plenty and diverse as well. In addition to investigating stochastic low-frequency variability, one may attempt to look at determining physical properties of only Wolf-Rayet candidates which are eclipsing binaries similar to Southworth and Bowman (2022)'s approach. Polarimetric measurements of Galactic WR stars's can also shed light onto how Wolf-Rayet binaries interact, understanding their complex wind structures and how clumping or colliding winds work as well (Hubrig et al., 2020). Studies of effects of multiplicity and their evolution leading up to them becoming black hole progenitors (Sen et al., 2021; Sander et al., 2019) are also of utmost importance, given the frequency of binarity within massive star systems or even how often they end up in multiple systems (Dsilva et al., 2020, 2022).

Chapter 5

Conclusions

Adhering to the primary goal of characterising the optical variability of Wolf-Rayet stars, I have produced an overview analysis onto a sample of 58 bright Wolf-Rayet stars using TESS 2-minute cadence data. I have adopted and modified the semi-Lorentzian function used by Bowman et al. (2019), adding an additional Cauchy distribution term as an attempt to locate the maximum peak, and to use this combined form as a fitting model for each star's unique Lomb-Scargle periodograms. I managed to extract all six best-fit parameters involved in this combined function for each available light curves of each star, and compiled them into a detailed table sorted in terms of Wolf-Rayet sub-classes (Table. C).

Due to a limited amount of time available, my analysis has grinded to a halt before any further steps can be taken. However, the prospects of analysis stemming from this newfound wealth of data is vast. The next immediate step is to be able to compare all of the obtained numerical parameters against the WRs stellar parameters (such as stellar mass, luminosity, band-filter magnitudes, etc..) and look for any correlations between them, akin to studies done by Bowman et al. (2019) or Lenoir-Craig et al. (2022). Additionally, for WRs which do not convey much useful information in their 2-minute cadence, it calls for further analysis utilising the longer 30-minute cadence data from their TESS FFI frames. All in order to more accurately decipher and characterise their naturally convoluted variability.

Appendix A

Figures of Wolf-Rayet Stars' Light Curves and Power Spectrum Fit

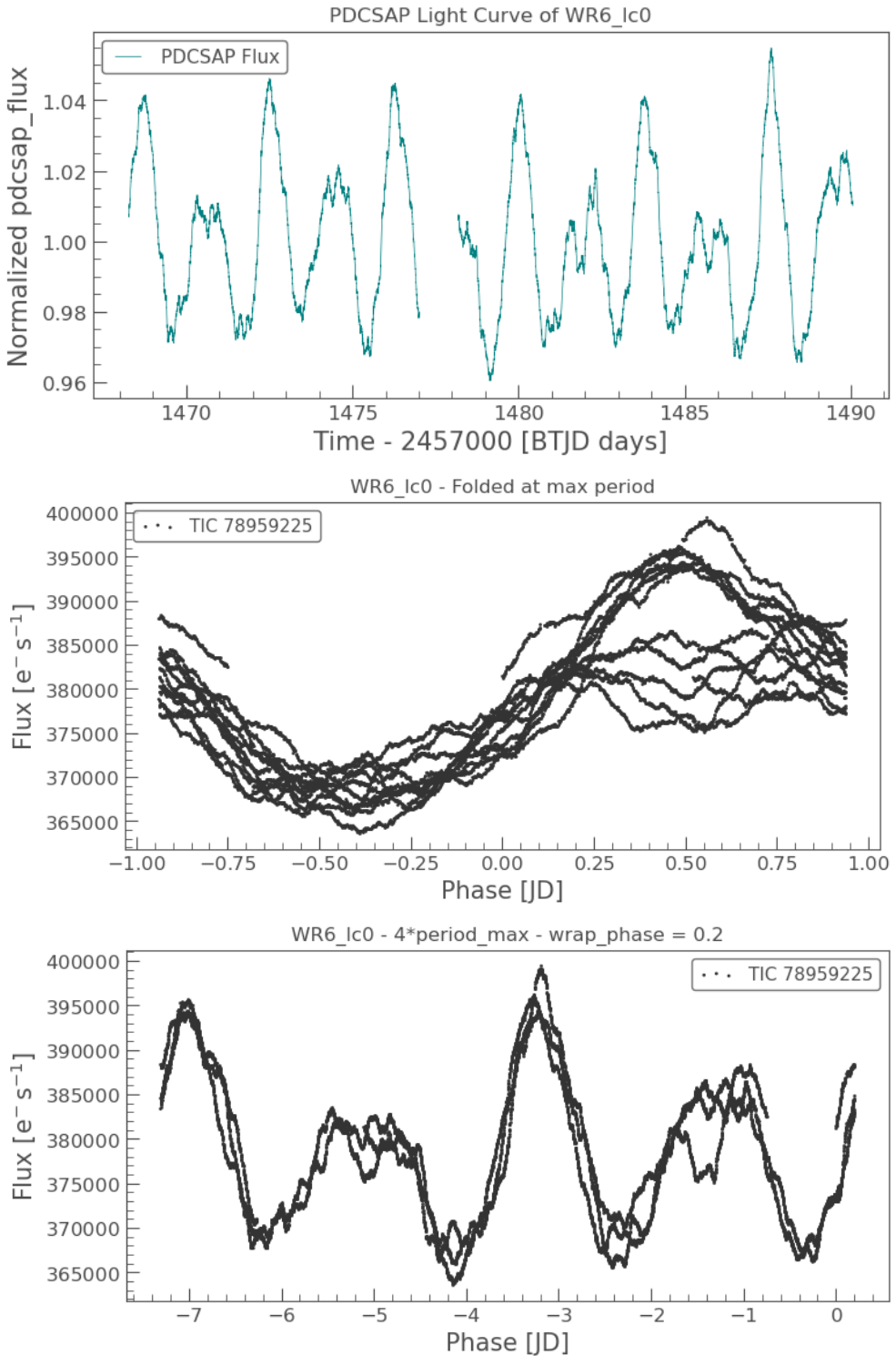

Figure A.1: WR6 light curve data: (*top to bottom*) PDCSAP flux, max period fold, 4-times-max-period with 0.2 wrapping phase

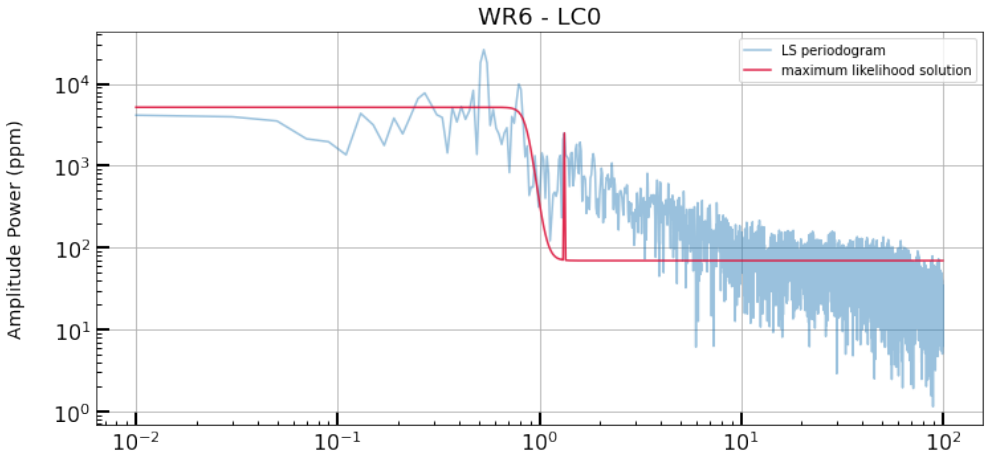
WR6 - LC0
LS periodogram
maximum likelihood solution
Amplitude Power (ppm)

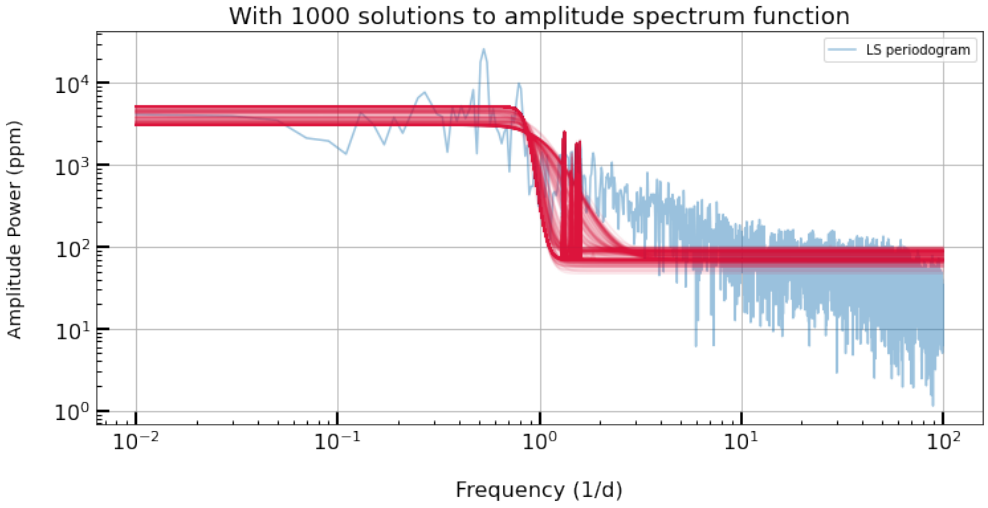
With 1000 solutions to amplitude spectrum function
LS periodogram
Amplitude Power (ppm)
Frequency (1/d)

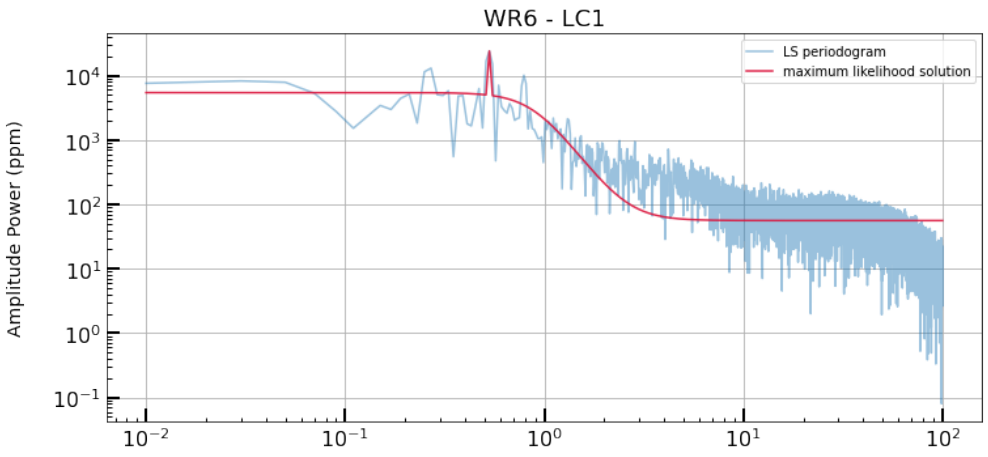
WR6 - LC1
LS periodogram
maximum likelihood solution
Amplitude Power (ppm)

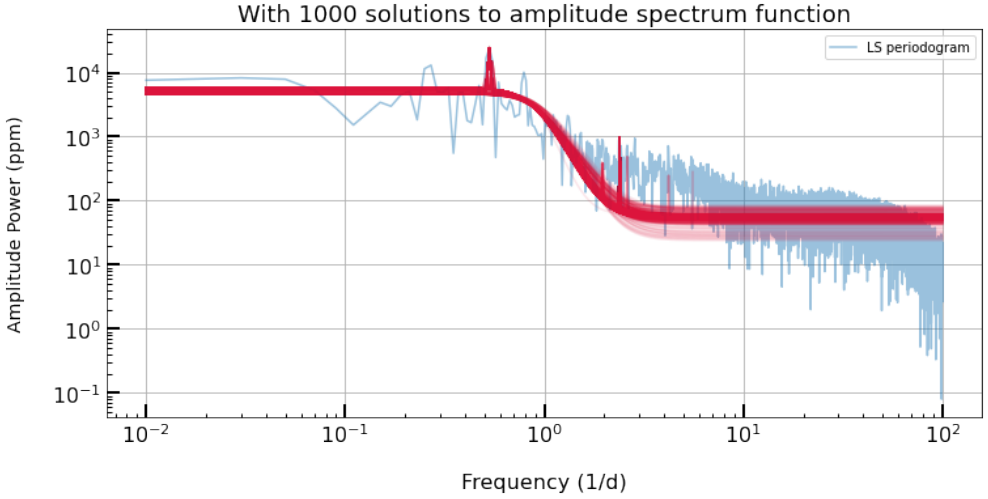
With 1000 solutions to amplitude spectrum function
LS periodogram
Amplitude Power (ppm)
Frequency (1/d)

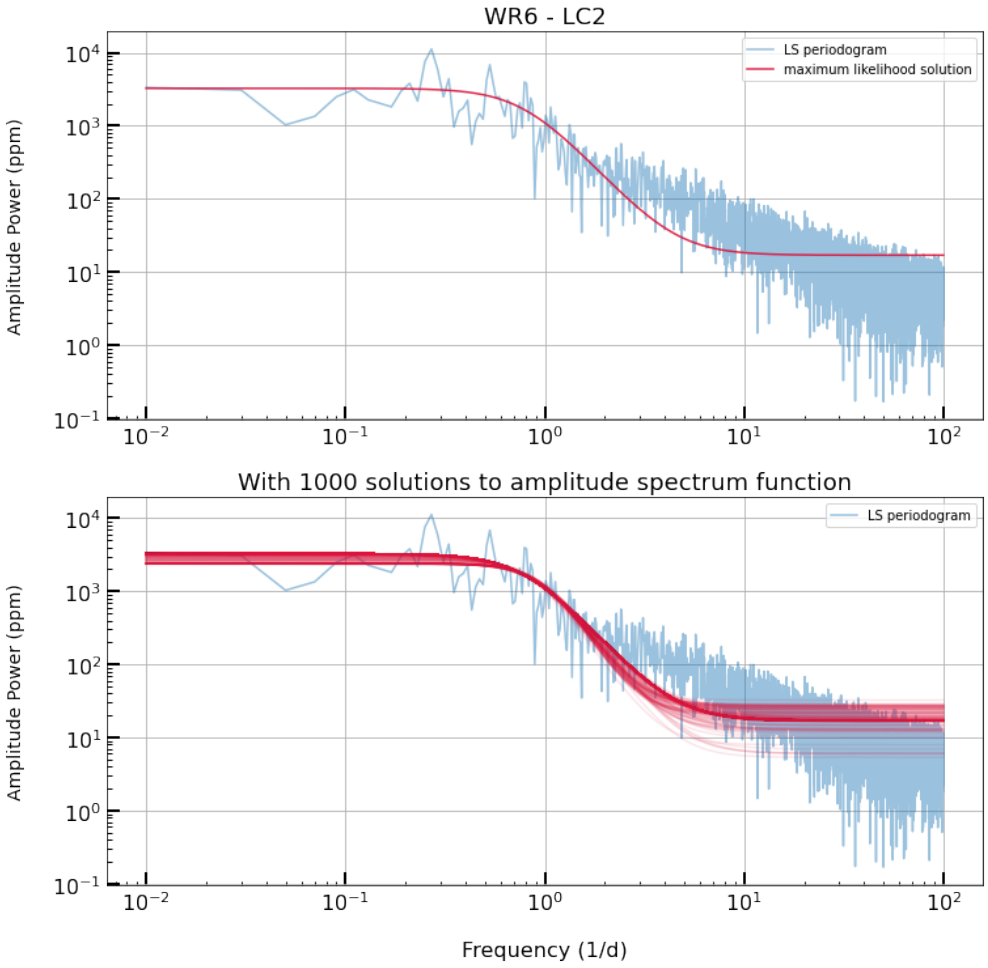

Figure A.2: MCMC amplitude spectrum + Cauchy distribution fits of WR6's Lomb-Scargle periodogram

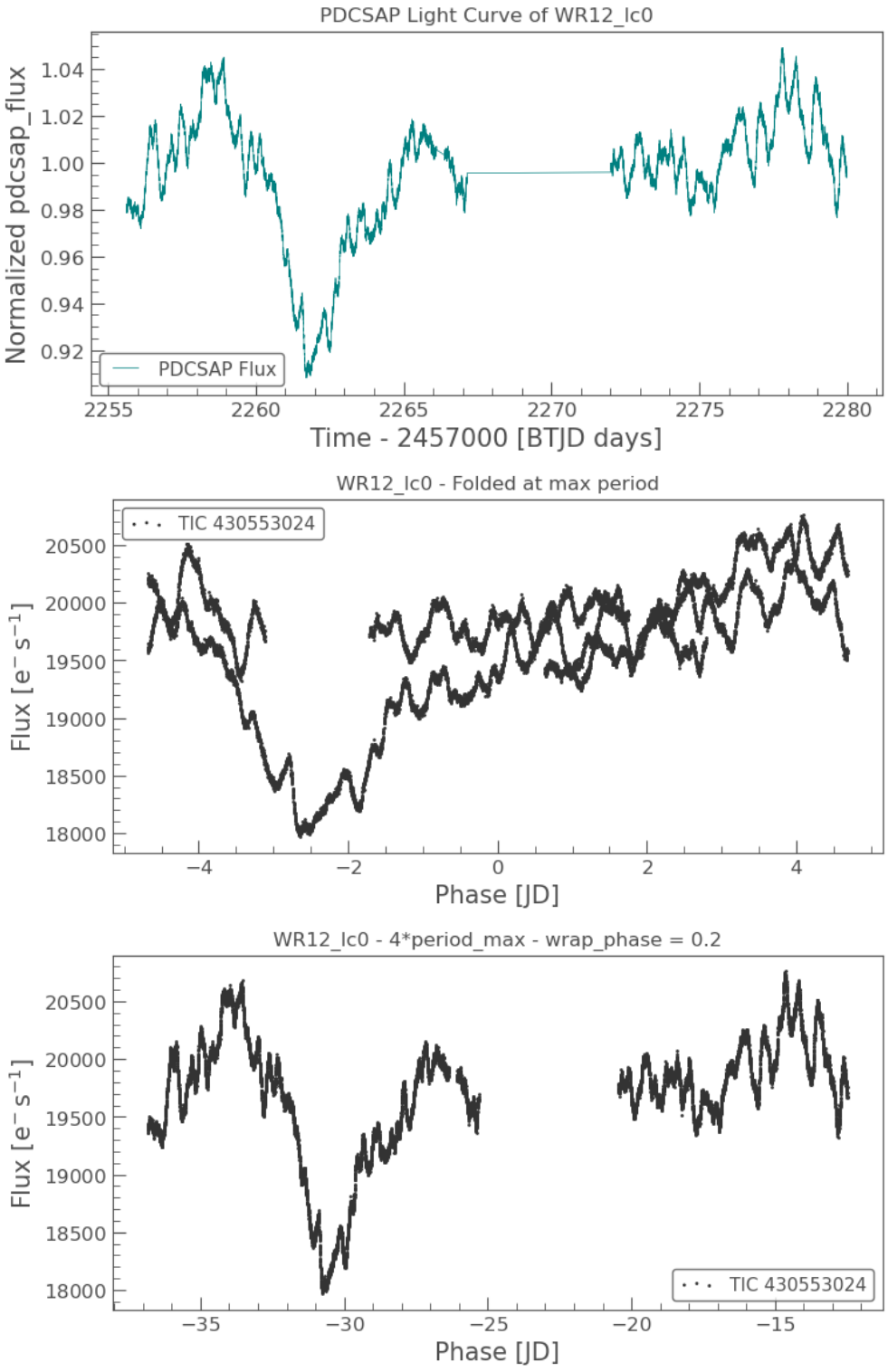

Figure A.3: WR12 light curve data: (*top to bottom*) PDCSAP flux, max period fold, 4-times-max-period with 0.2 wrapping phase

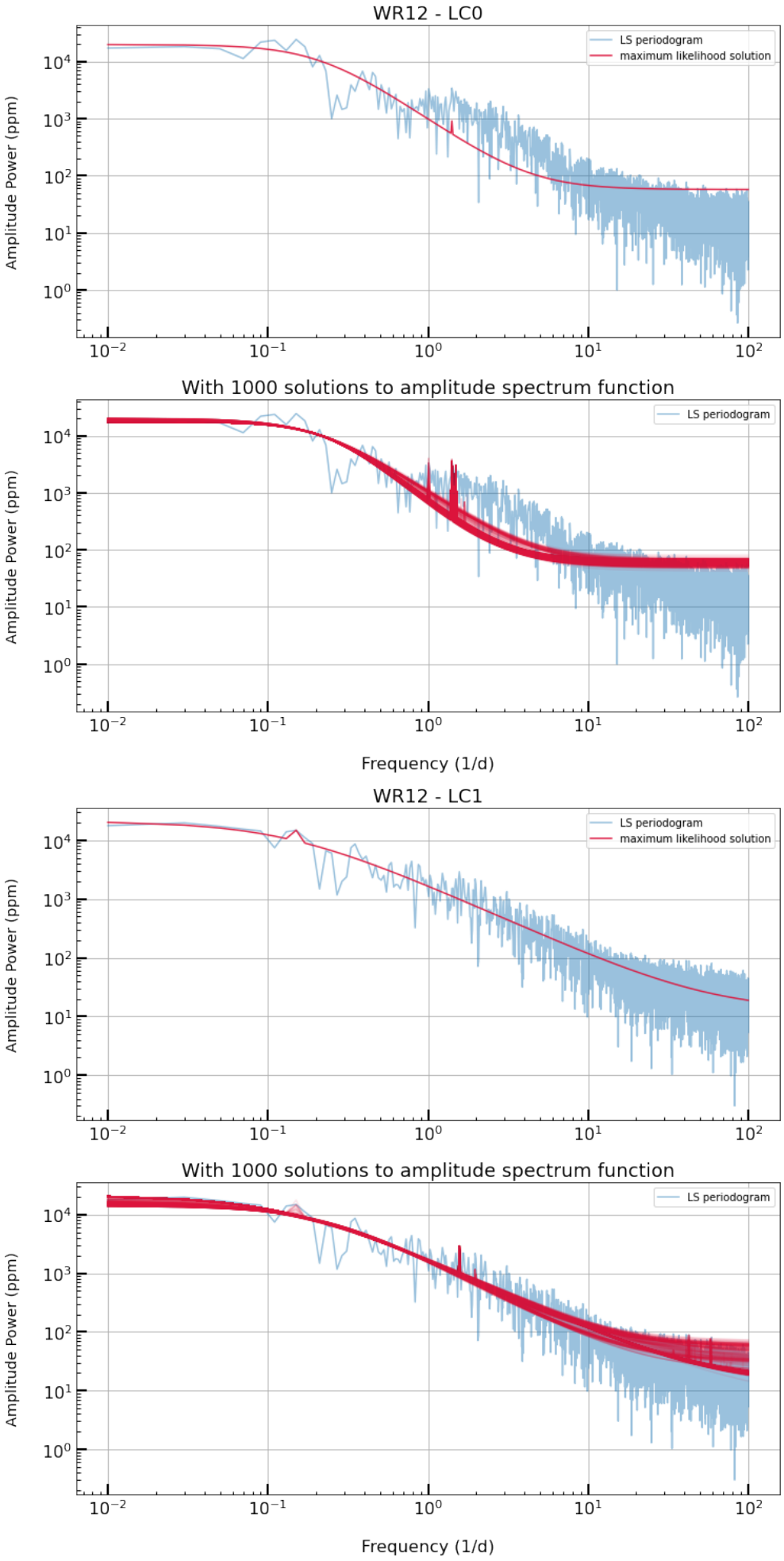

Figure A.4: MCMC amplitude spectrum + Cauchy distribution fits of WR12's Lomb-Scargle periodogram

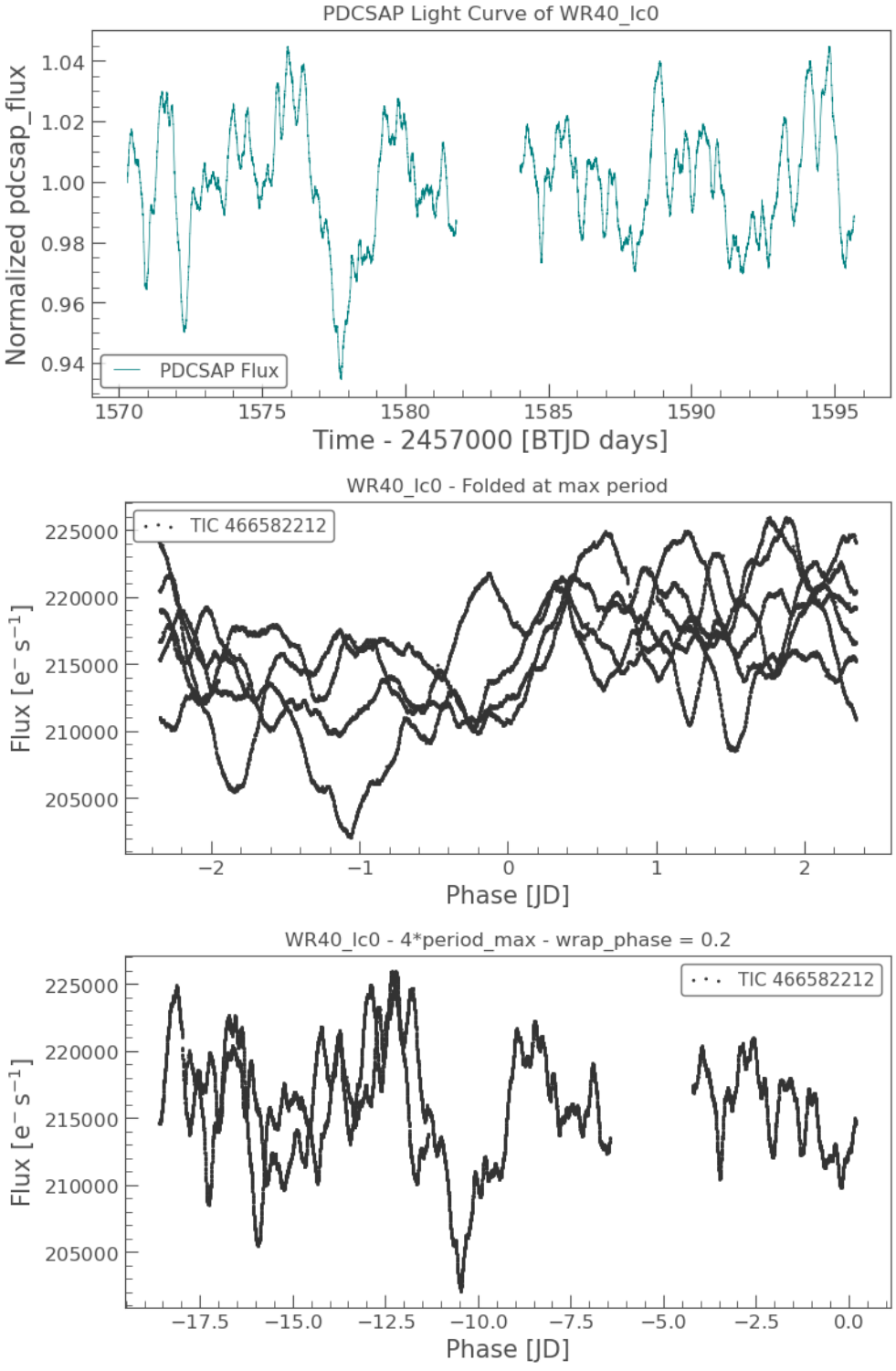

Figure A.5: WR40 light curve data: (*top to bottom*) PDCSAP flux, max period fold, 4-times-max-period with 0.2 wrapping phase

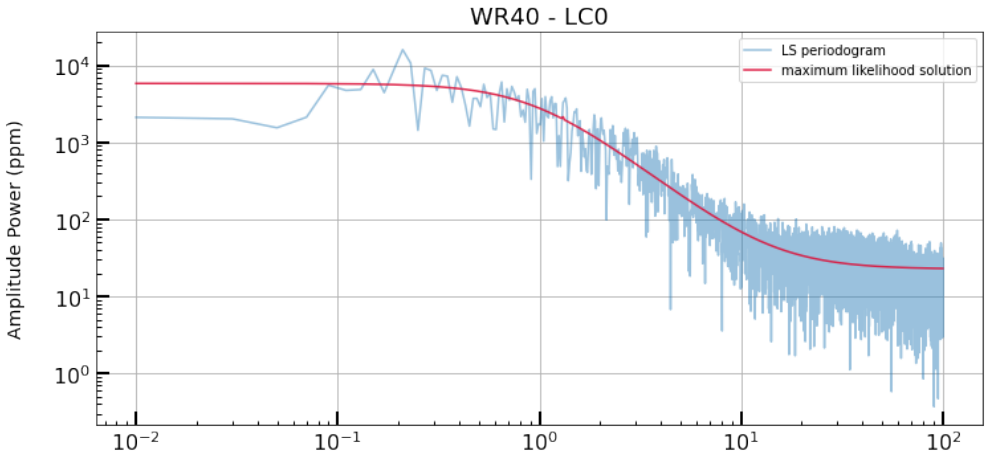
WR40 - LC0
LS periodogram
maximum likelihood solution
Amplitude Power (ppm)

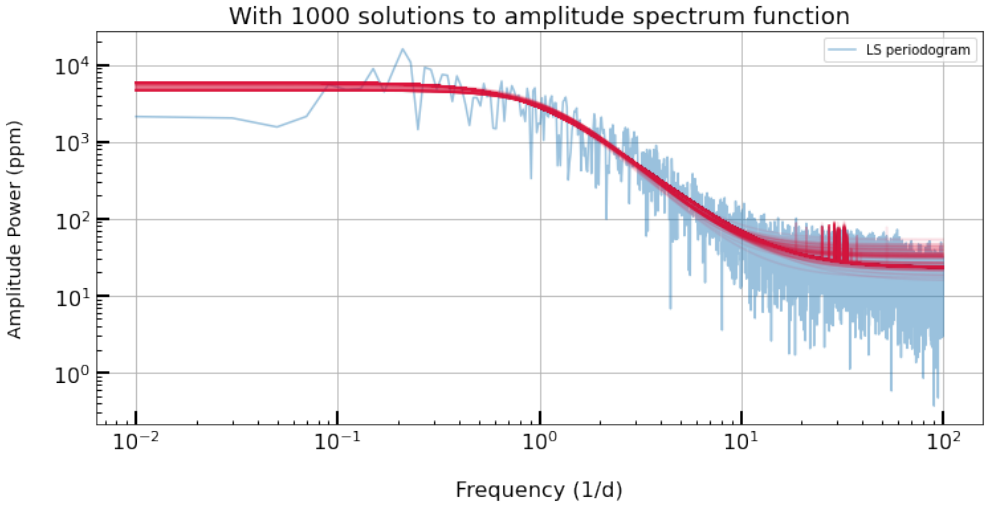
With 1000 solutions to amplitude spectrum function
LS periodogram
Amplitude Power (ppm)
Frequency (1/d)

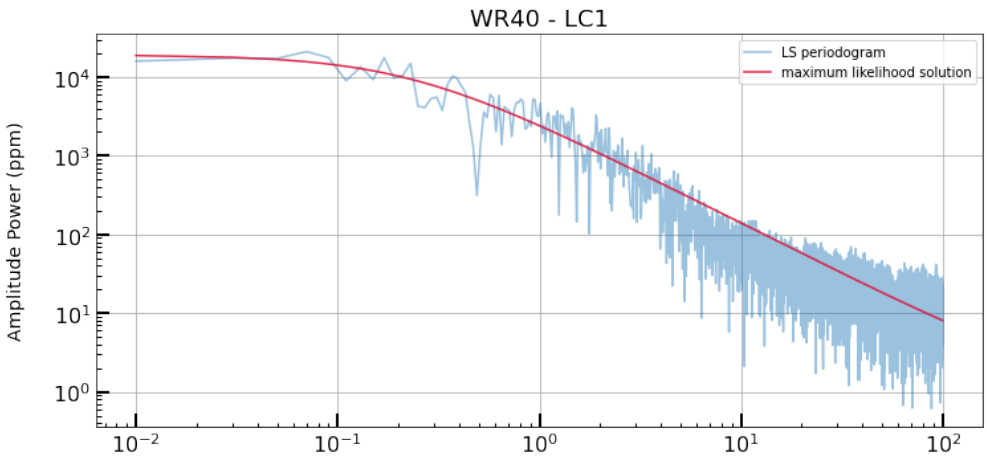
WR40 - LC1
LS periodogram
maximum likelihood solution
Amplitude Power (ppm)

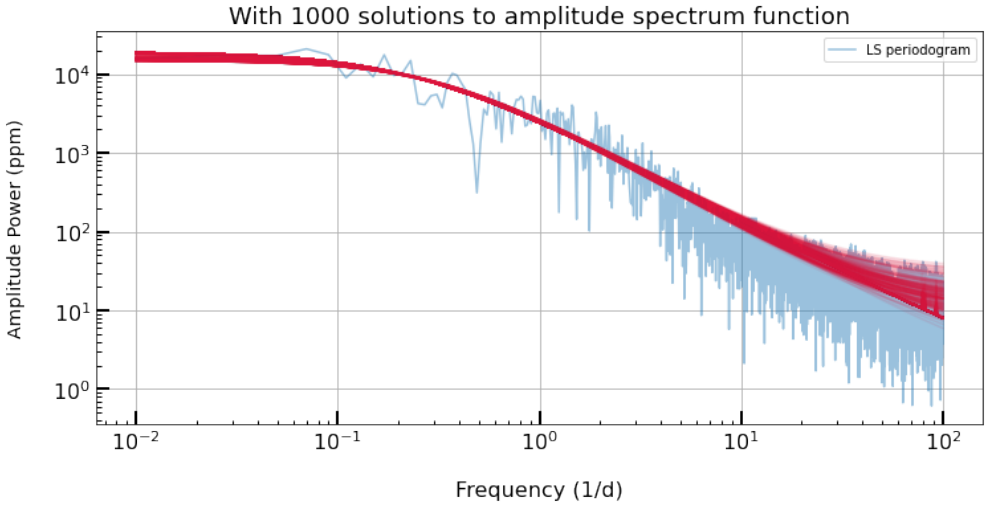
With 1000 solutions to amplitude spectrum function
LS periodogram
Amplitude Power (ppm)
Frequency (1/d)

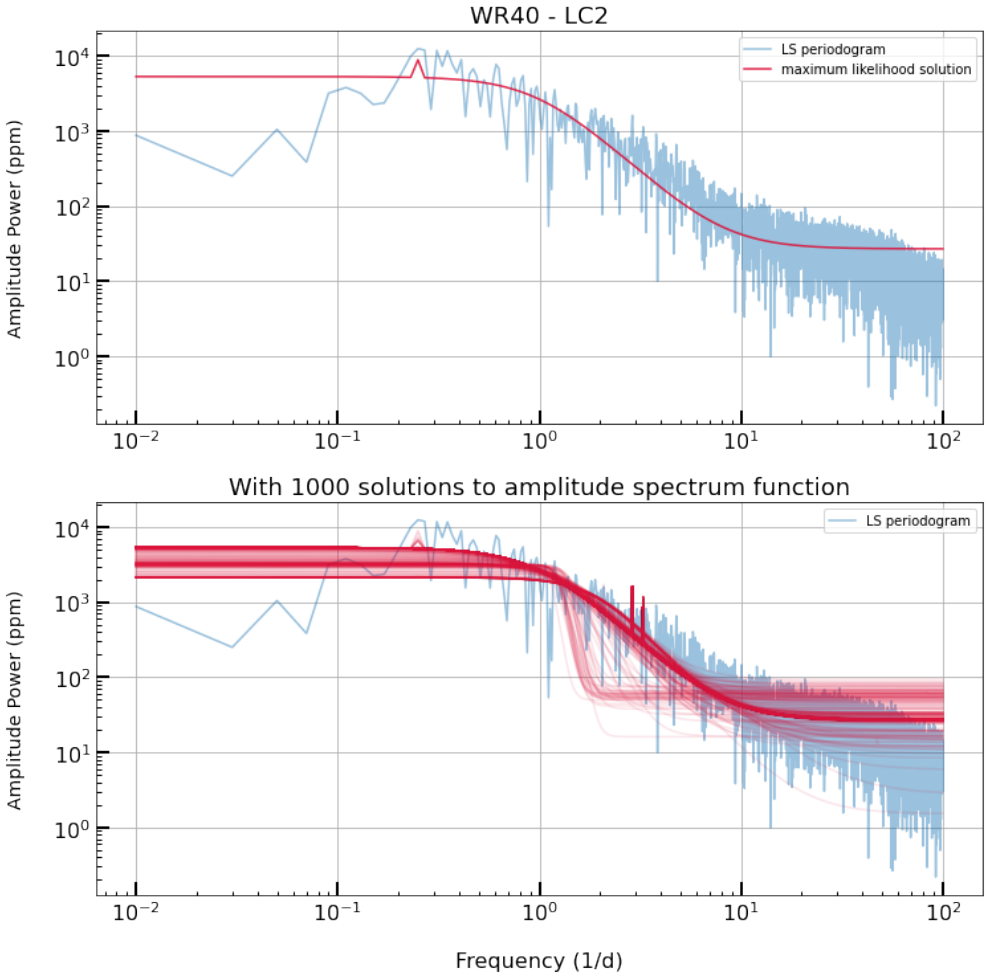

Figure A.6: MCMC amplitude spectrum + Cauchy distribution fits of WR40's Lomb-Scargle periodogram

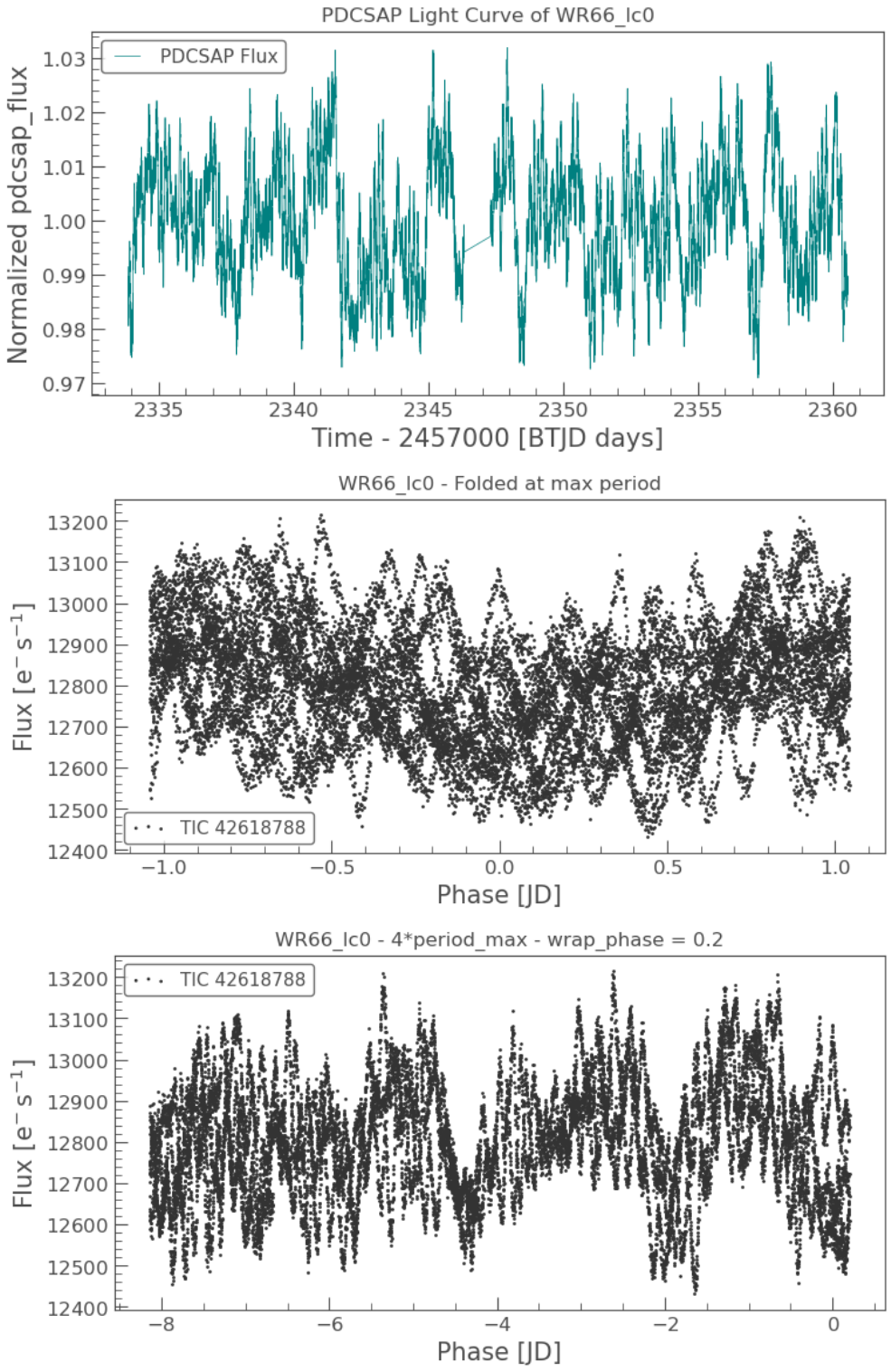

Figure A.7: WR66 light curve data: (*top to bottom*) PDCSAP flux, max period fold, 4-times-max-period with 0.2 wrapping phase

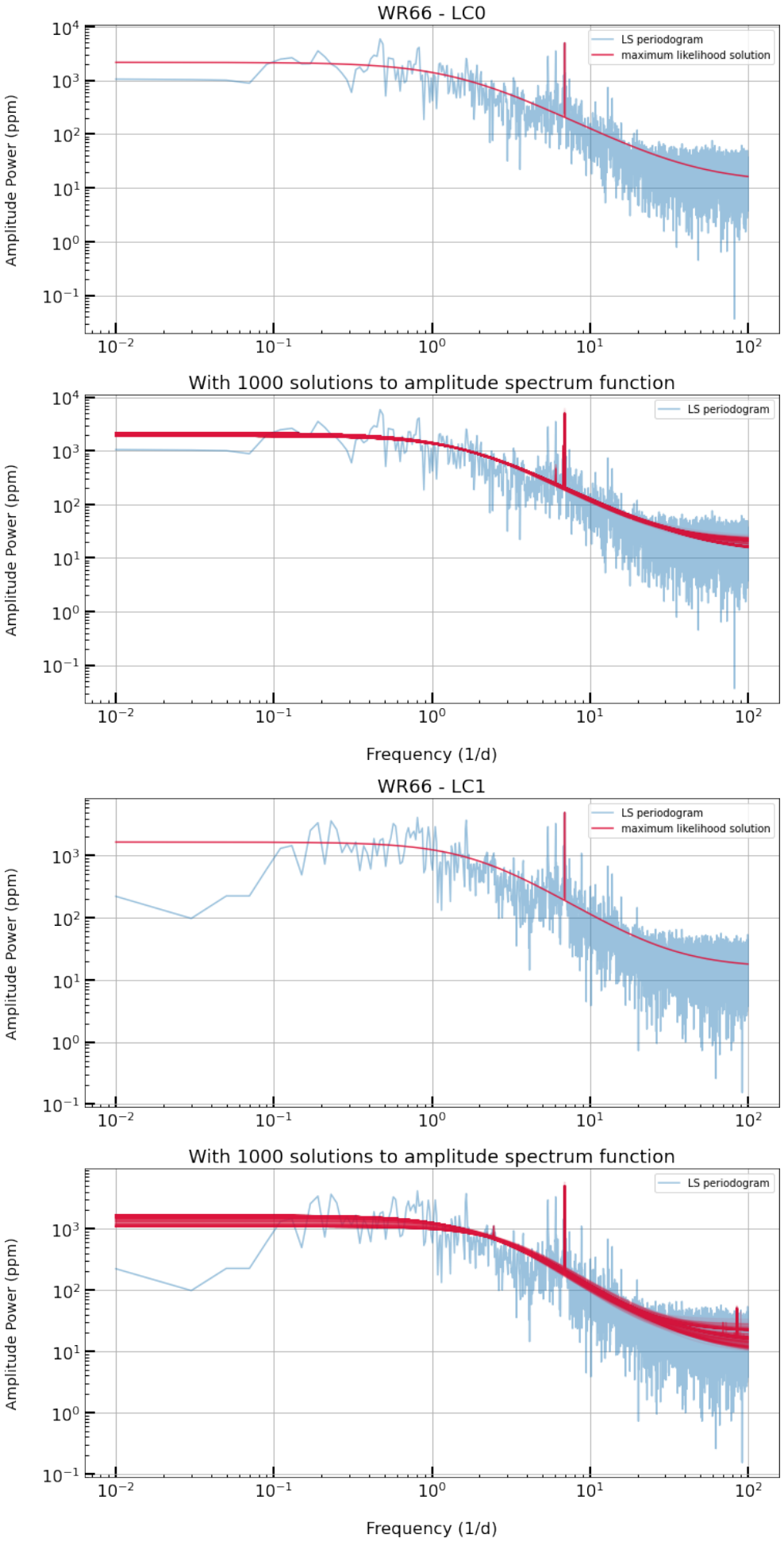

Figure A.8: MCMC amplitude spectrum + Cauchy distribution fits of WR66's Lomb-Scargle periodogram

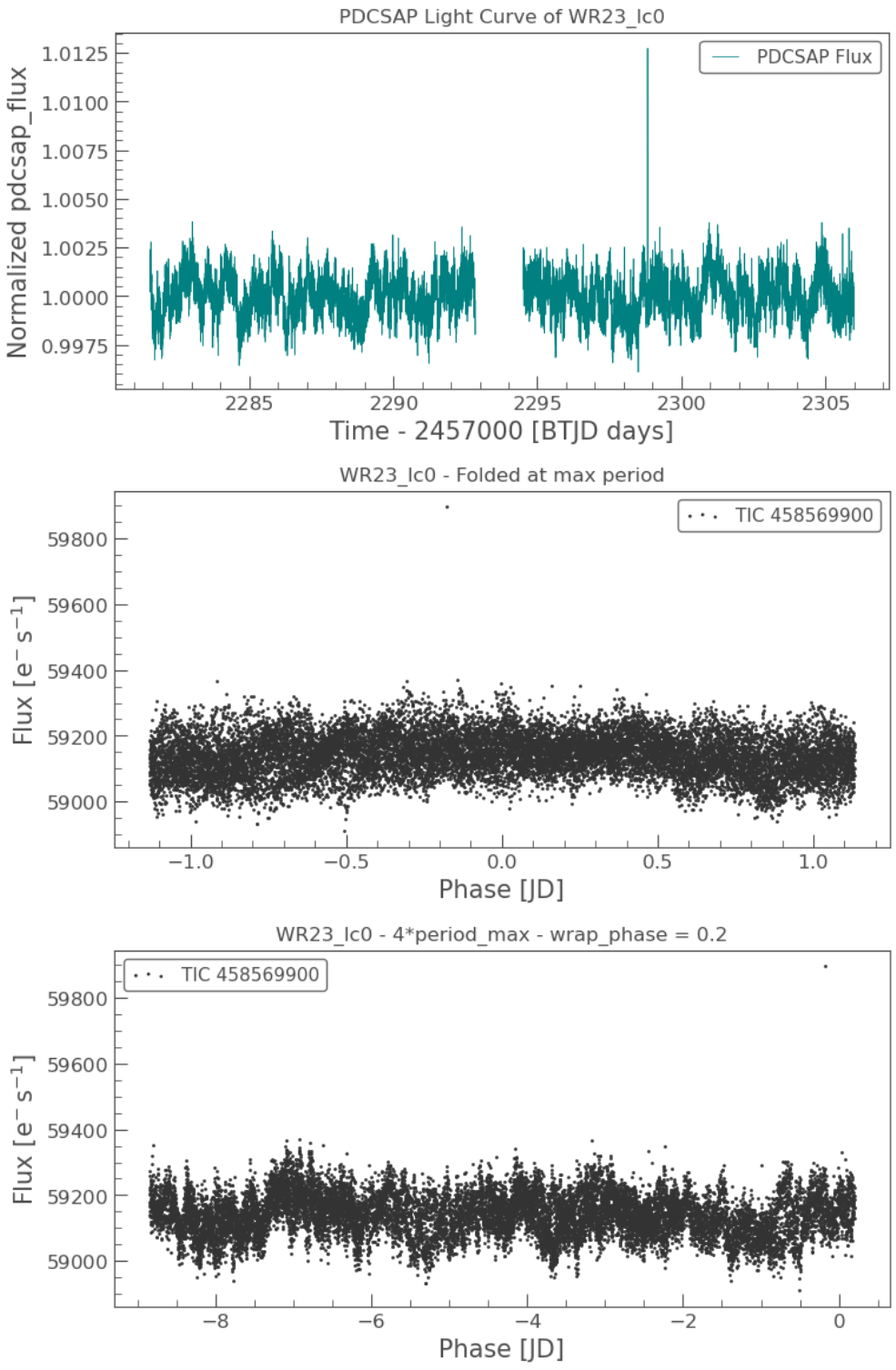

Figure A.9: WR23 light curve data: (*top to bottom*) PDCSAP flux, max period fold, 4-times-max-period with 0.2 wrapping phase

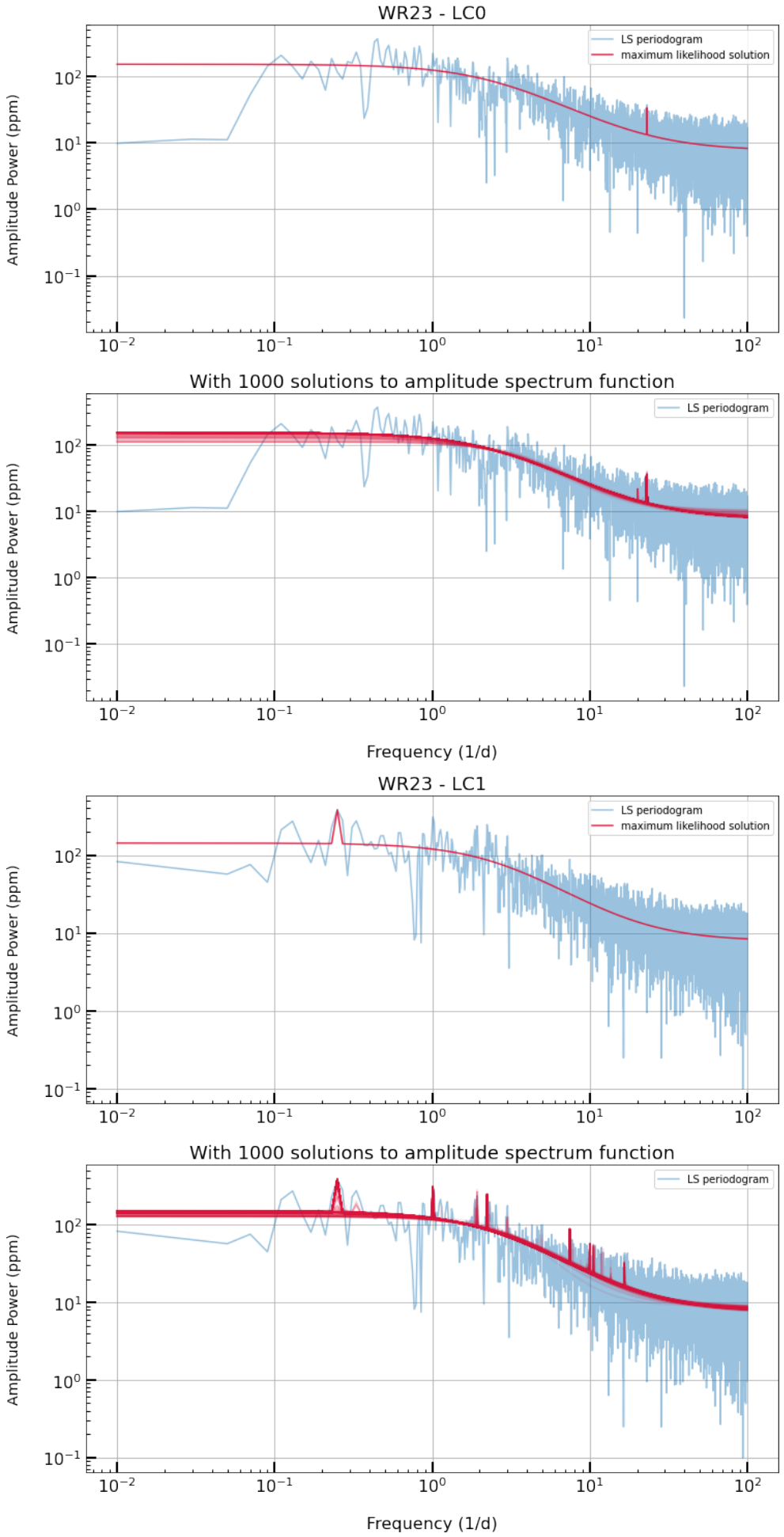

Figure A.10: MCMC amplitude spectrum + Cauchy distribution fits of WR23's Lomb-Scargle periodogram

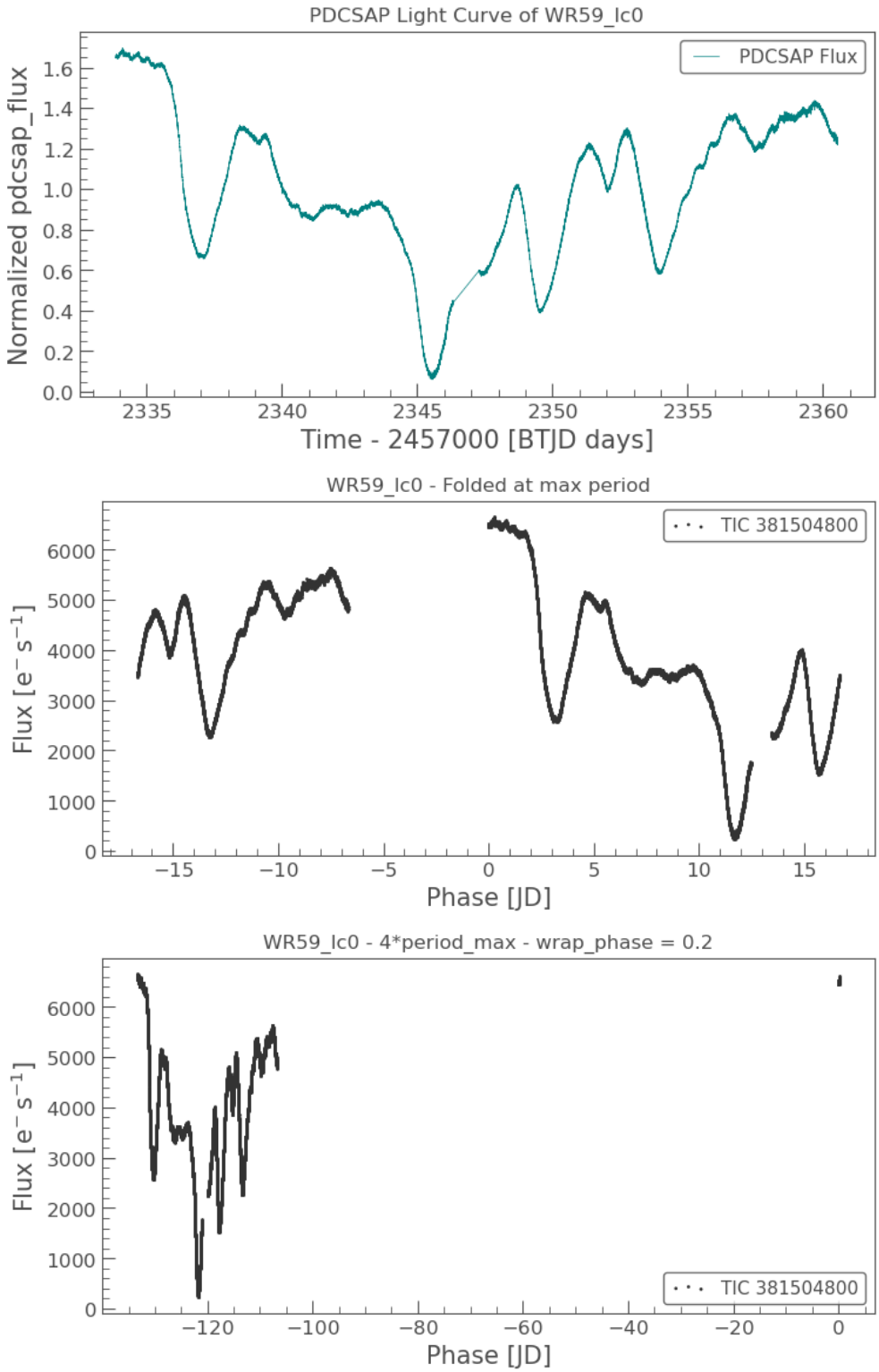

Figure A.11: WR59 light curve data: (*top to bottom*) PDCSAP flux, max period fold, 4-times-max-period with 0.2 wrapping phase

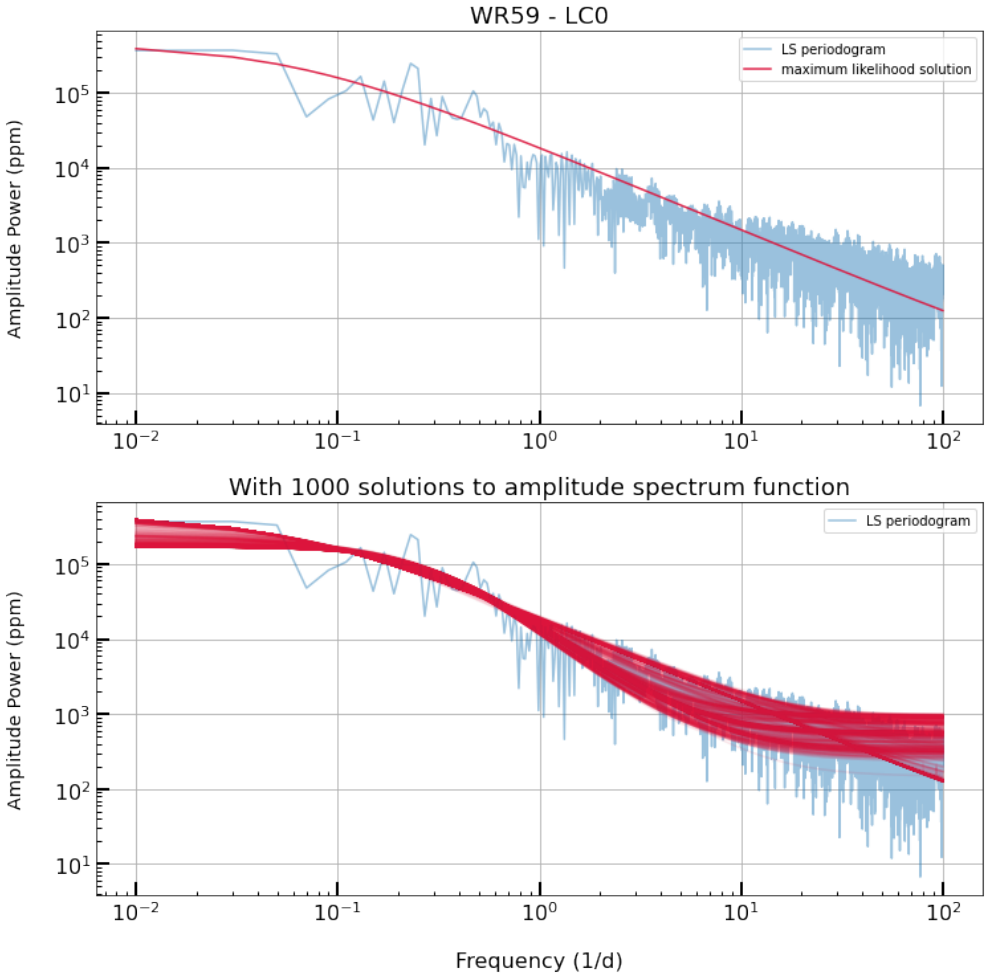

Figure A.12: MCMC amplitude spectrum + Cauchy distribution fits of WR59's Lomb-Scargle periodogram

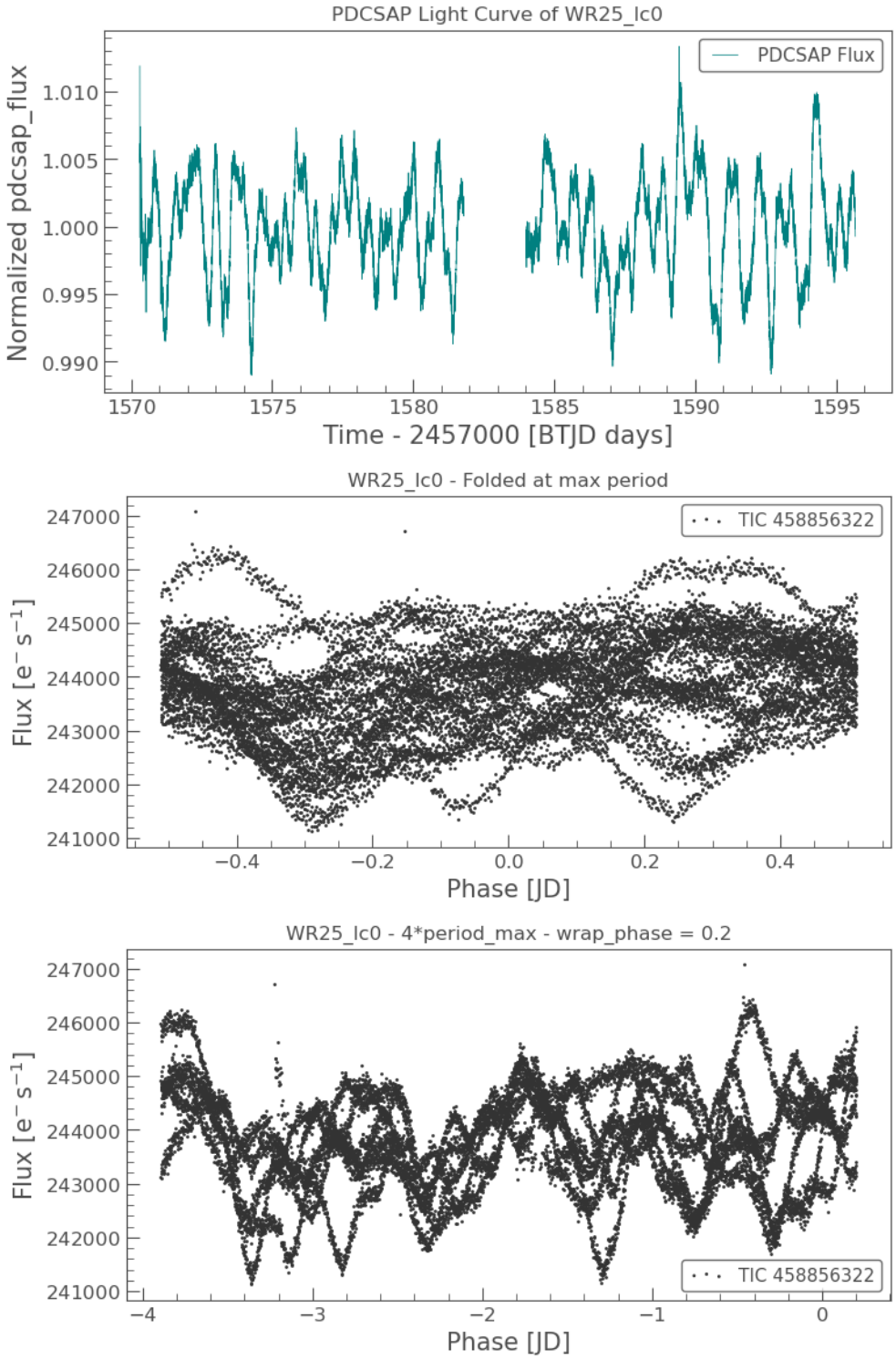

Figure A.13: WR25 light curve data: (*top to bottom*) PDCSAP flux, max period fold, 4-times-max-period with 0.2 wrapping phase

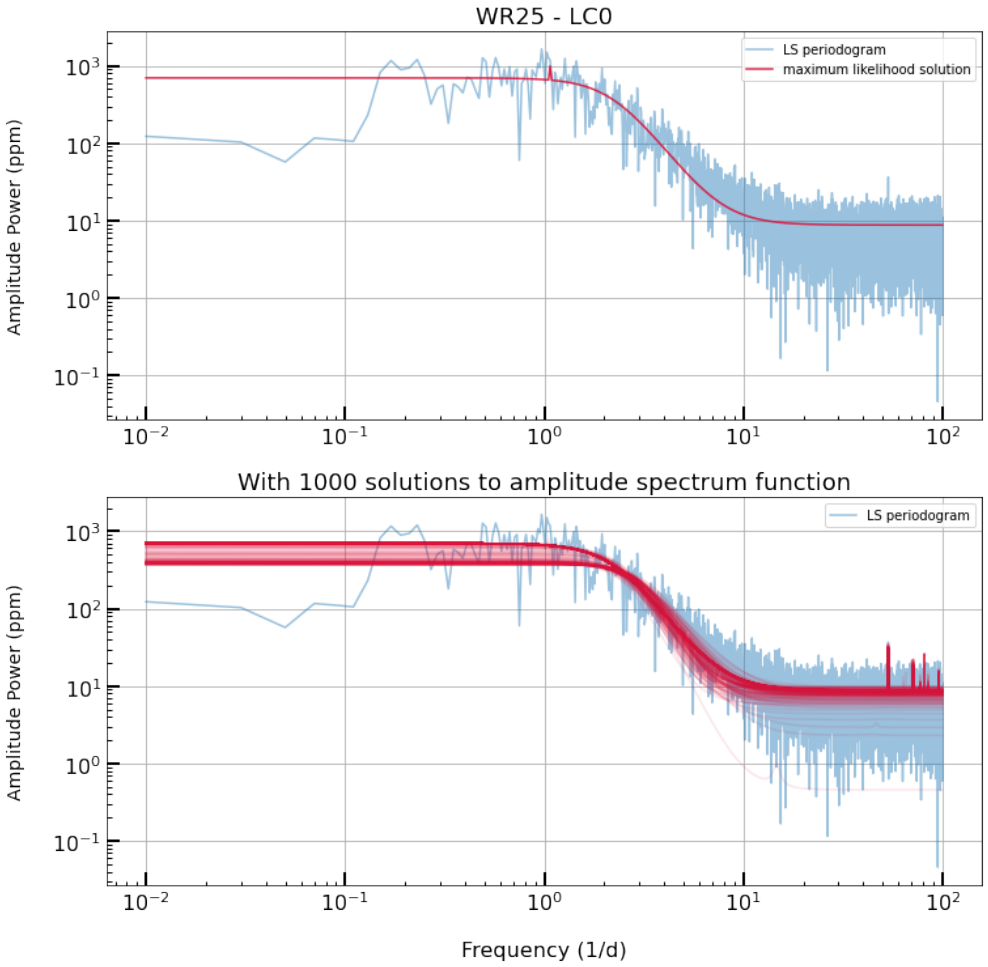
WR25 - LC0
LS periodogram
maximum likelihood solution
Amplitude Power (ppm)
With 1000 solutions to amplitude spectrum function
LS periodogram
Amplitude Power (ppm)
Frequency (1/d)

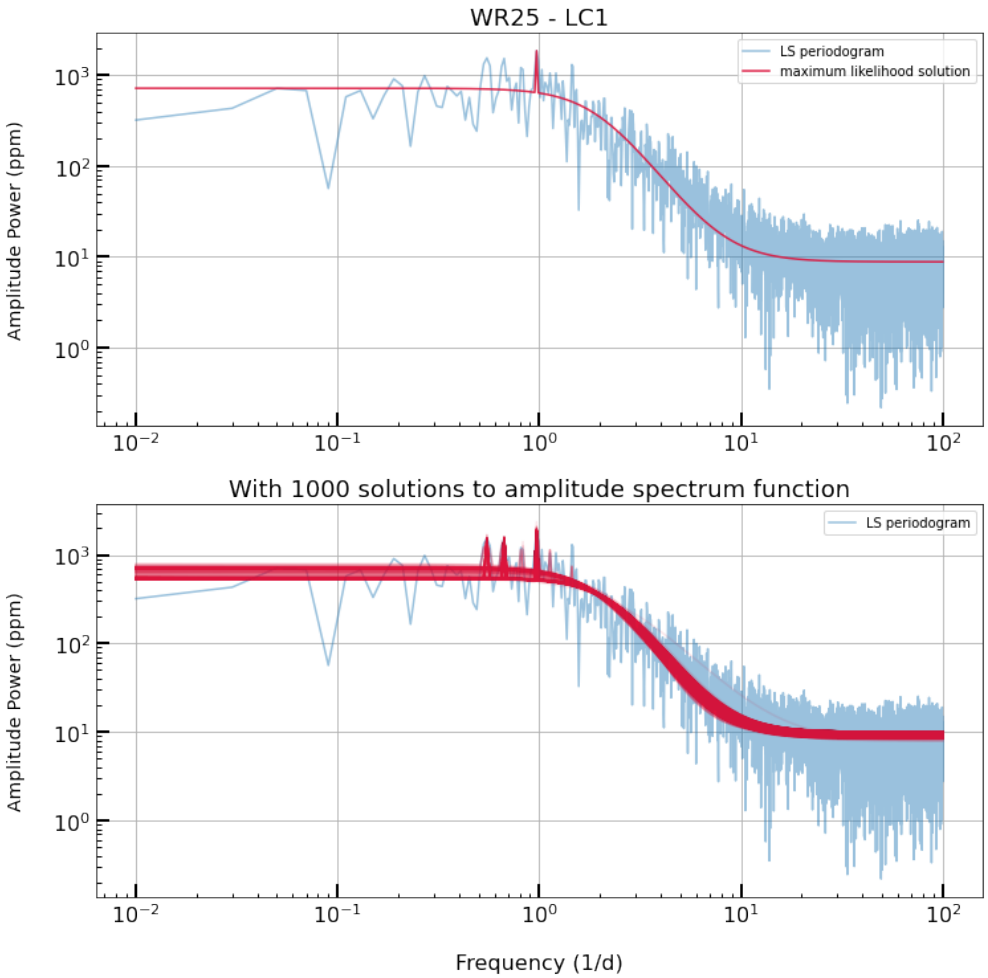
WR25 - LC1
LS periodogram
maximum likelihood solution
Amplitude Power (ppm)
With 1000 solutions to amplitude spectrum function
LS periodogram
Amplitude Power (ppm)
Frequency (1/d)

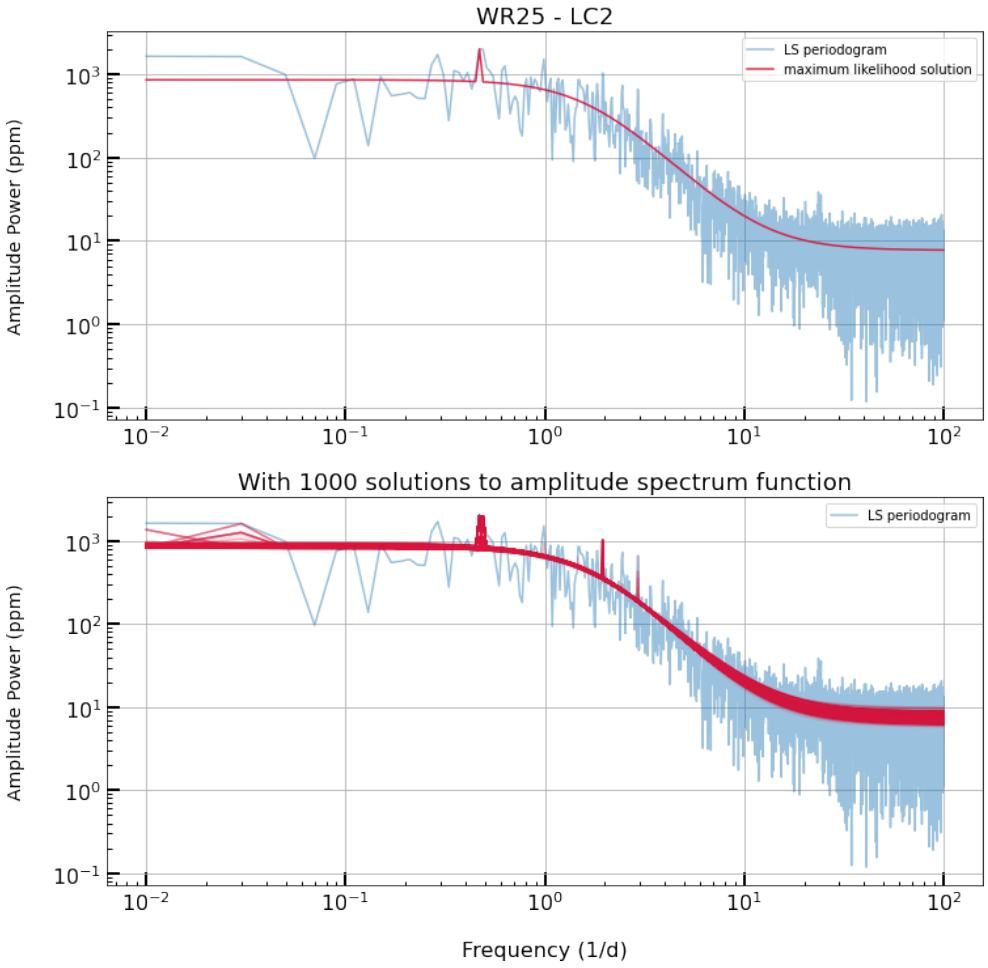

Figure A.14: MCMC amplitude spectrum + Cauchy distribution fits of WR25's Lomb-Scargle periodogram

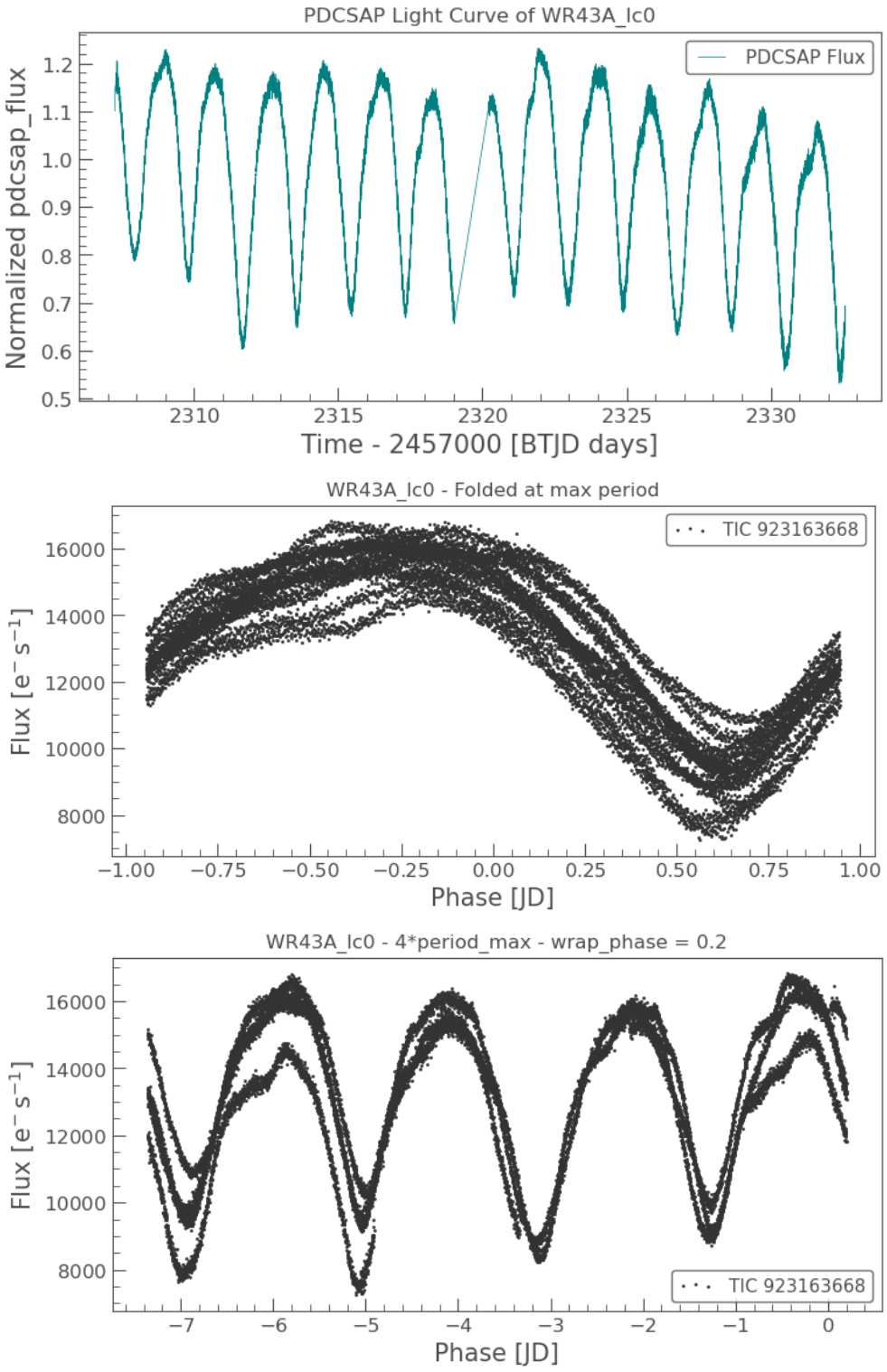

Figure A.15: WR43A, B, C light curve data: (*top to bottom*) PDCSAP flux, max period fold, 4-times-max-period with 0.2 wrapping phase

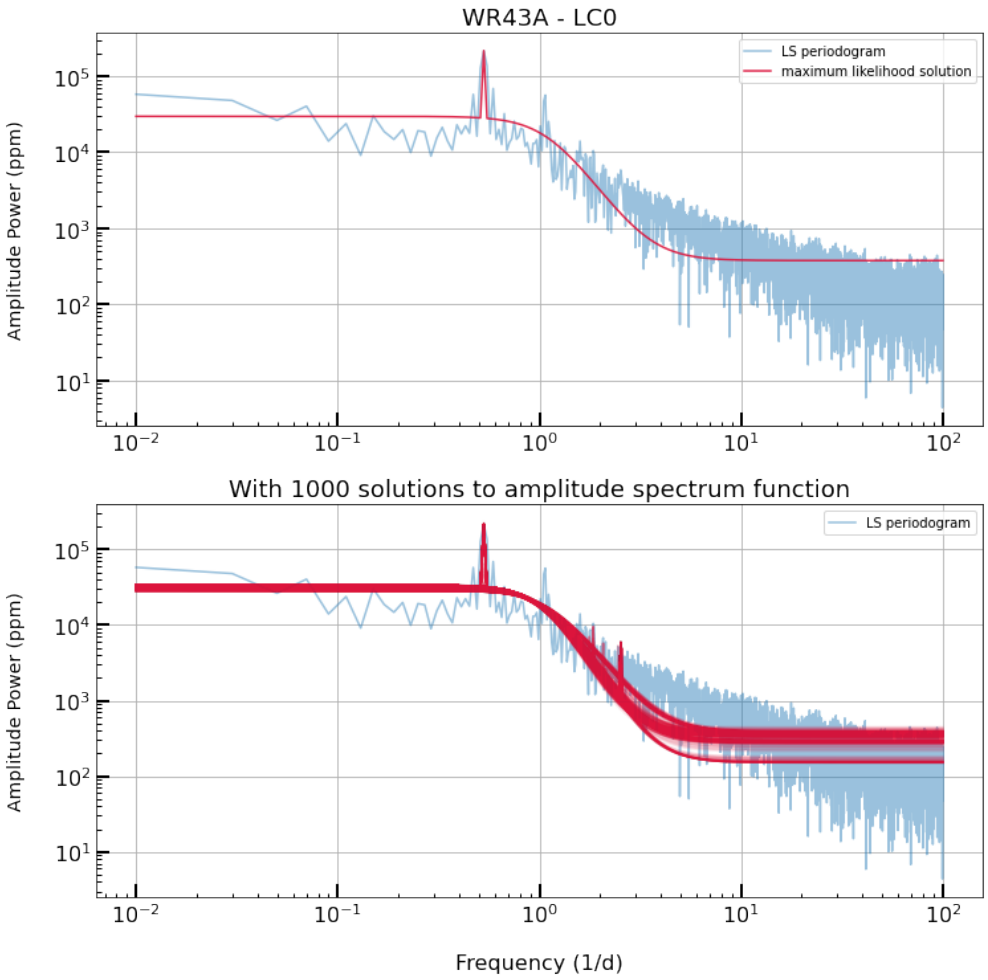

Figure A.16: MCMC amplitude spectrum + Cauchy distribution fits of WR43A, B, C's Lomb-Scargle periodogram

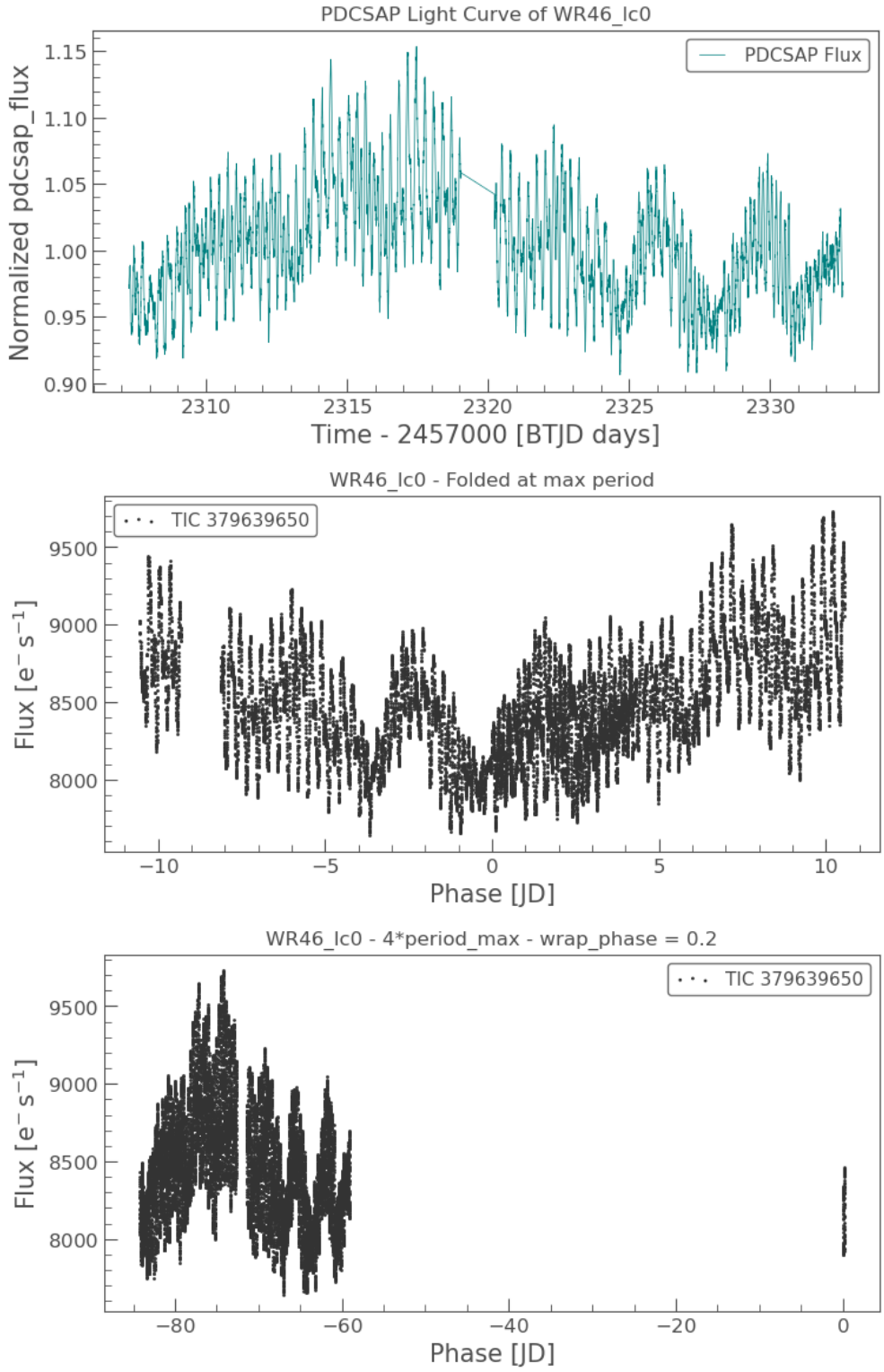

Figure A.17: WR46 light curve data: (*top to bottom*) PDCSAP flux, max period fold, 4-times-max-period with 0.2 wrapping phase

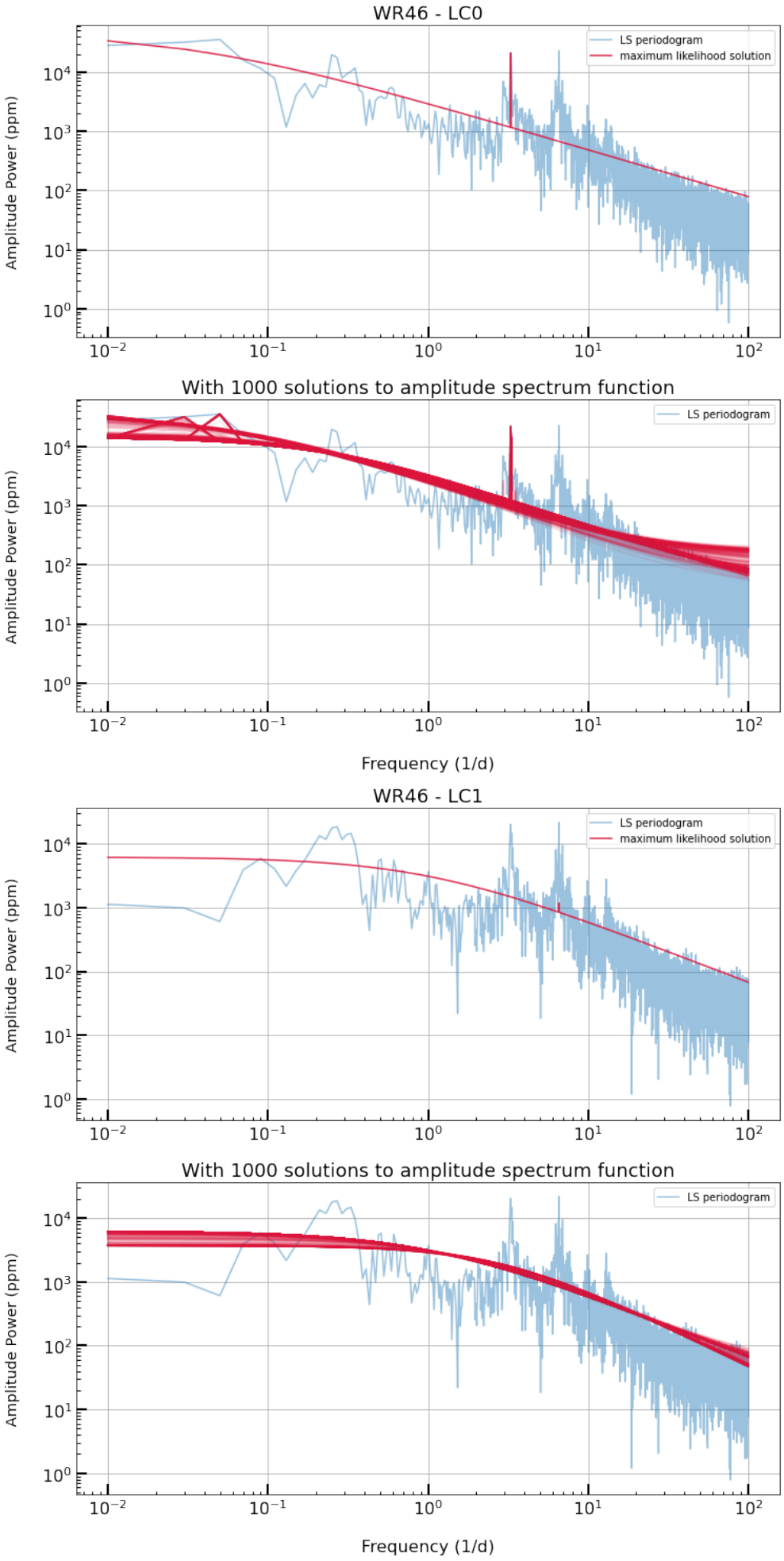

Figure A.18: MCMC amplitude spectrum + Cauchy distribution fits of WR46's Lomb-Scargle periodogram

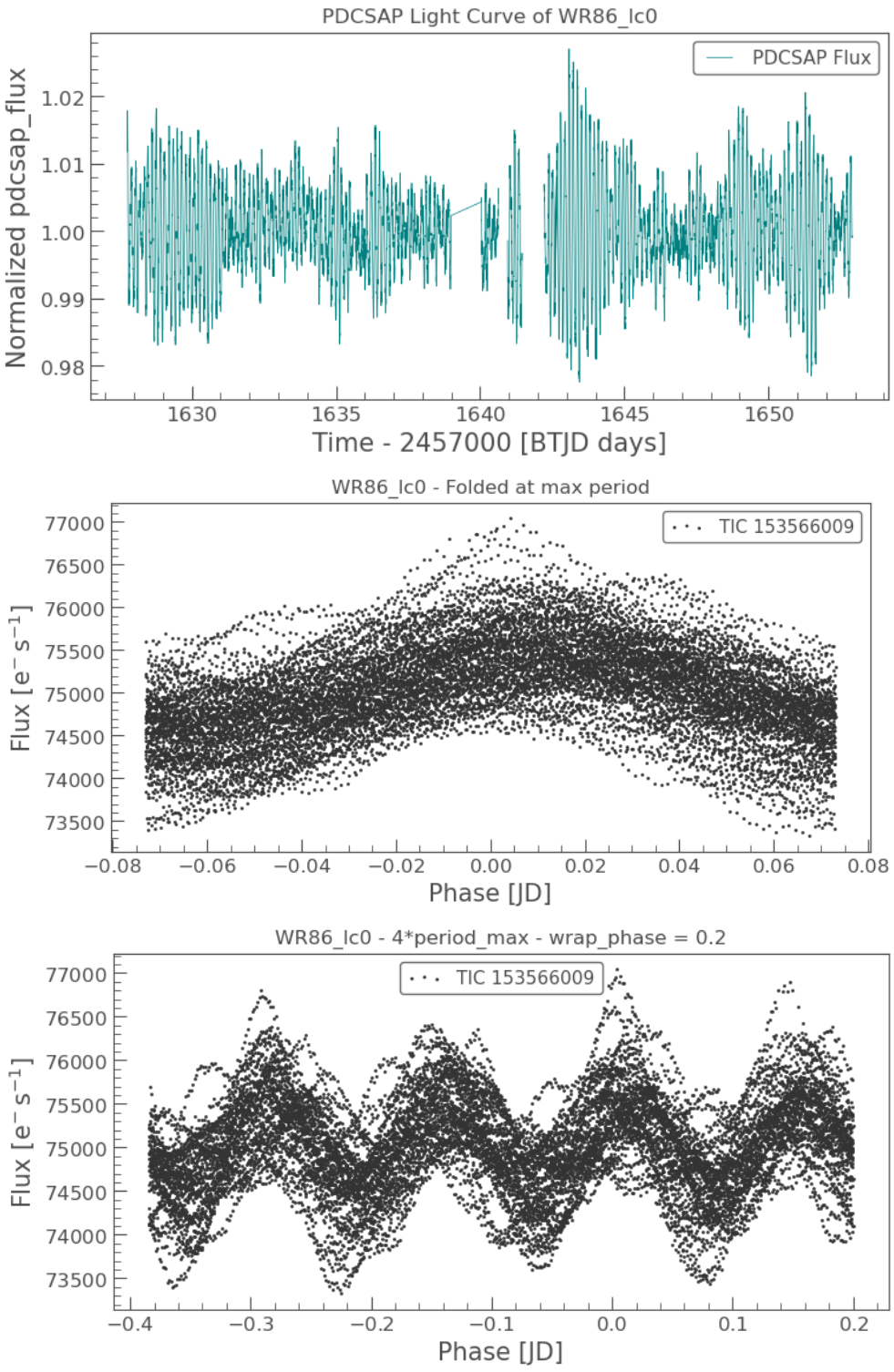

Figure A.19: WR86 light curve data: (*top to bottom*) PDCSAP flux, max period fold, 4-times-max-period with 0.2 wrapping phase

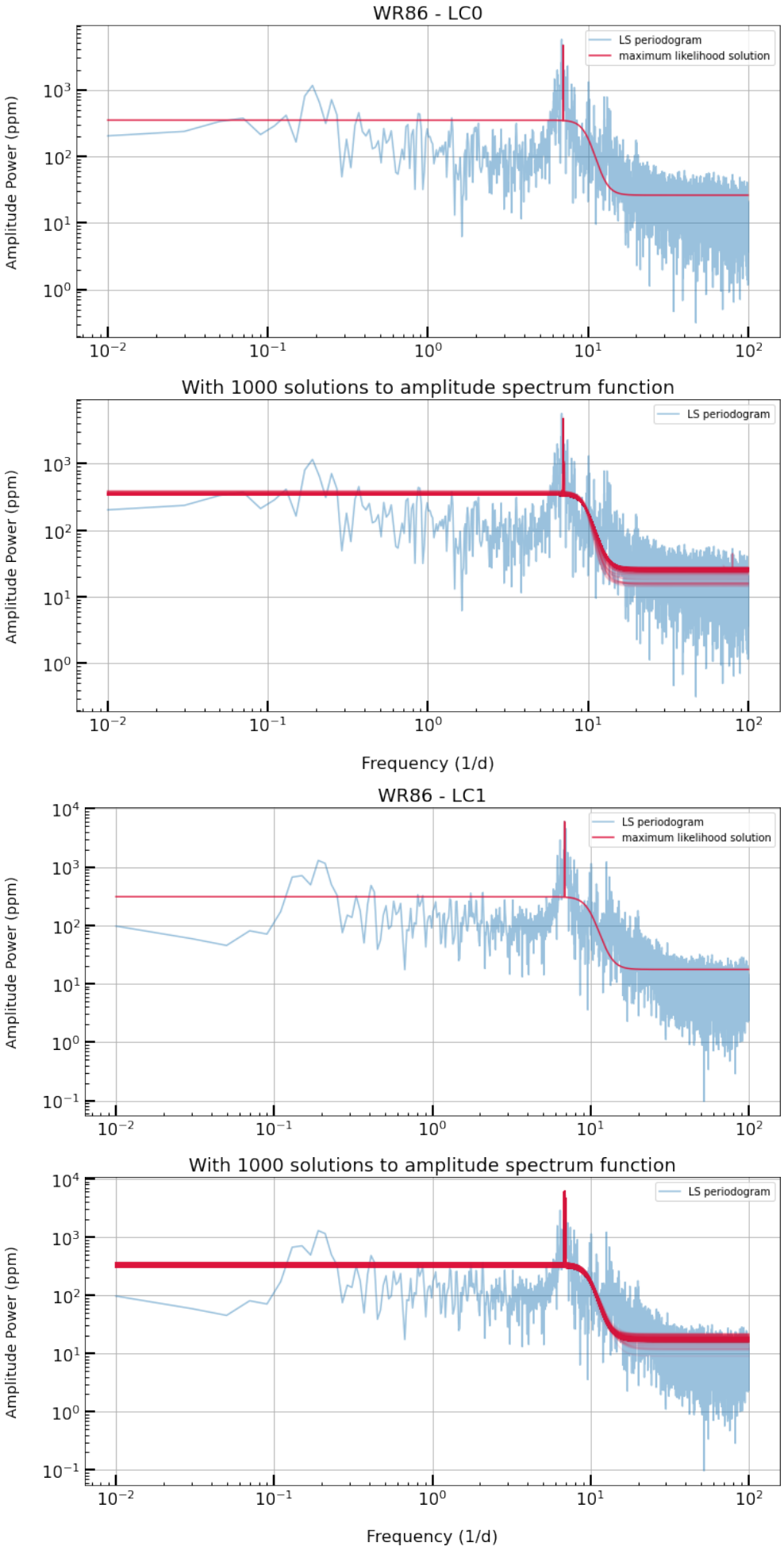

Figure A.20: MCMC amplitude spectrum + Cauchy distribution fits of WR86's Lomb-Scargle periodogram

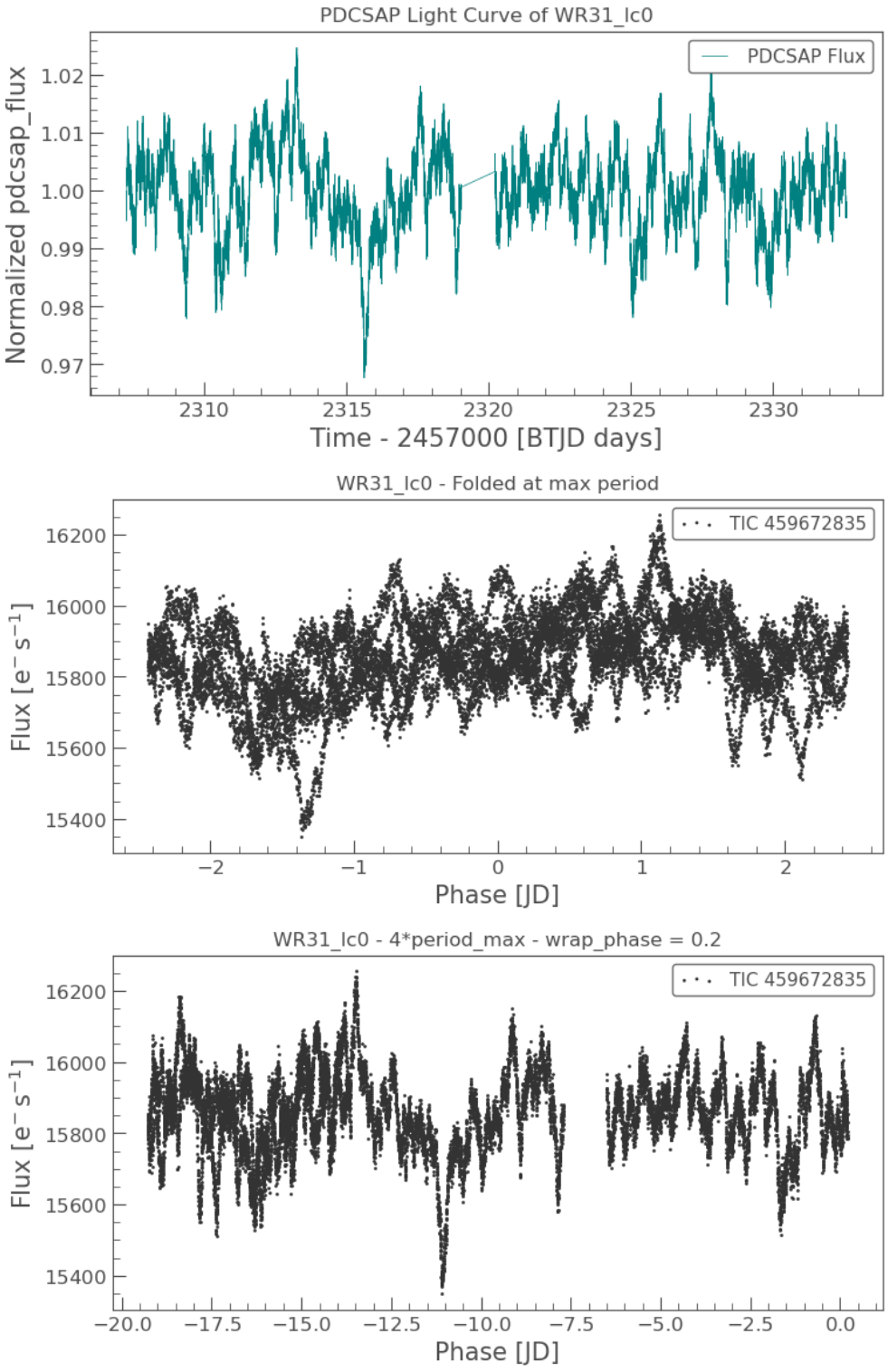

Figure A.21: WR31 light curve data: (*top to bottom*) PDCSAP flux, max period fold, 4-times-max-period with 0.2 wrapping phase

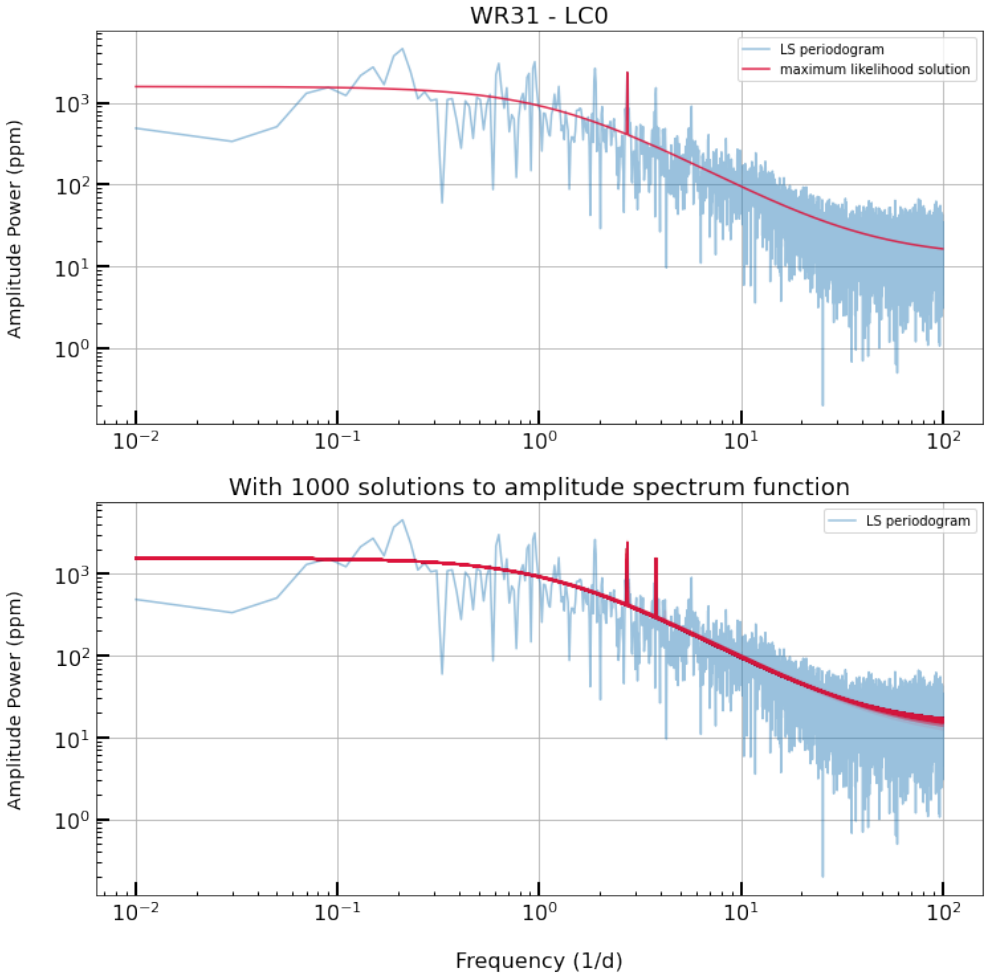

Figure A.22: MCMC amplitude spectrum + Cauchy distribution fits of WR31's Lomb-Scargle periodogram

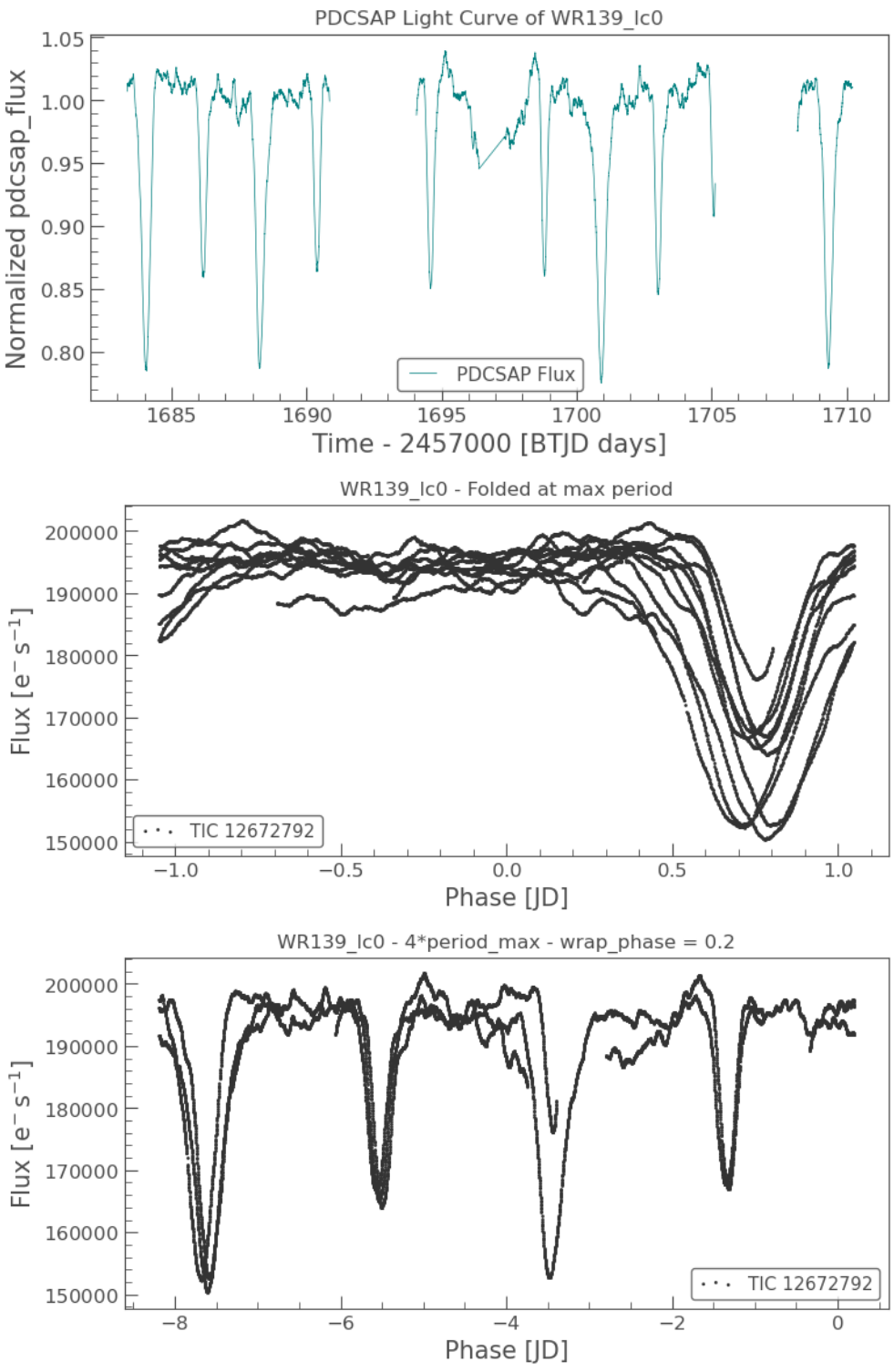

Figure A.23: WR139 light curve data: (*top to bottom*) PDCSAP flux, max period fold, 4-times-max-period with 0.2 wrapping phase

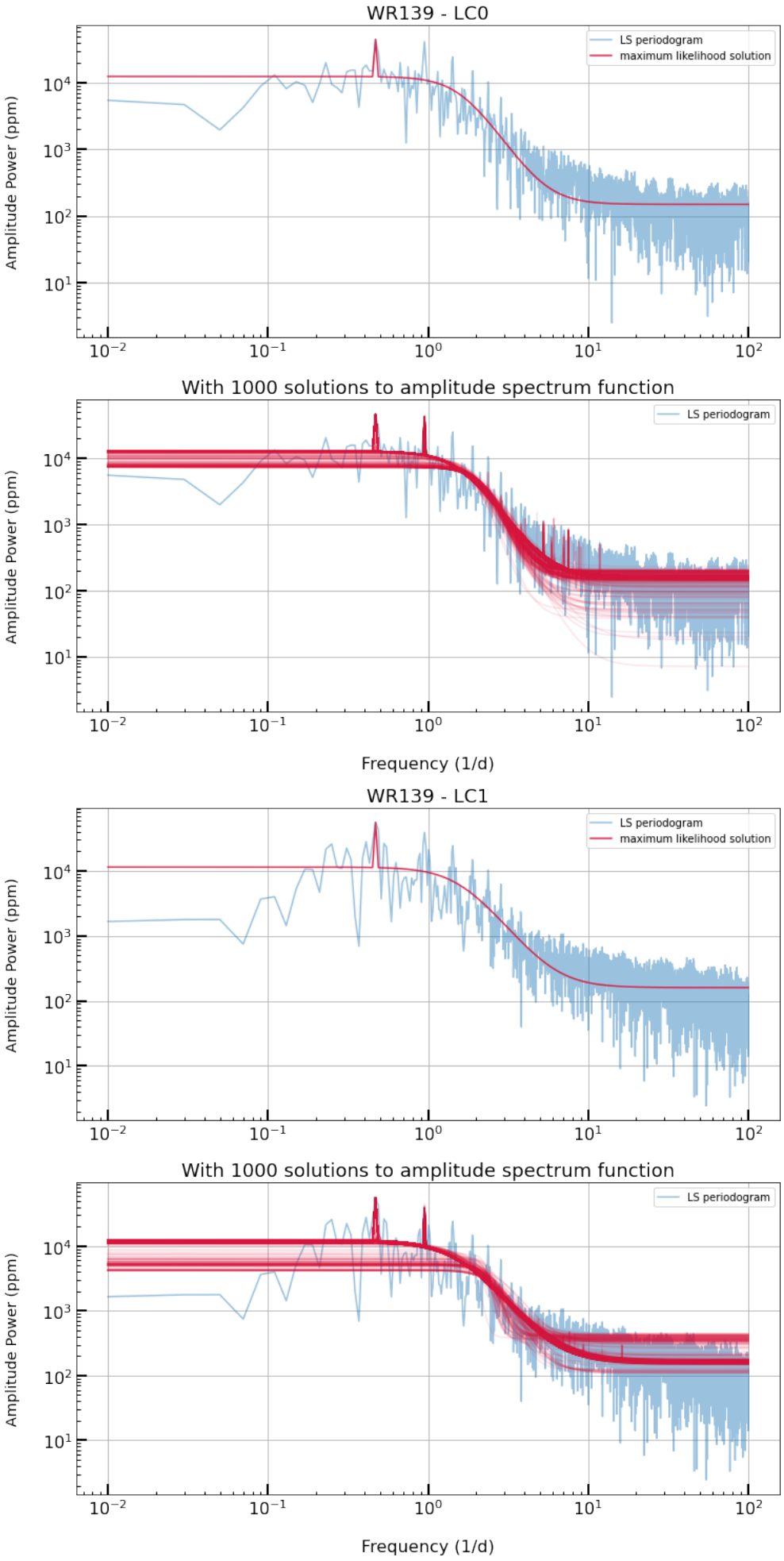
WR139 - LC0
LS periodogram
maximum likelihood solution
Amplitude Power (ppm)
With 1000 solutions to amplitude spectrum function
LS periodogram
Amplitude Power (ppm)
Frequency (1/d)
WR139 - LC1
LS periodogram
maximum likelihood solution
Amplitude Power (ppm)
With 1000 solutions to amplitude spectrum function
LS periodogram
Amplitude Power (ppm)
Frequency (1/d)

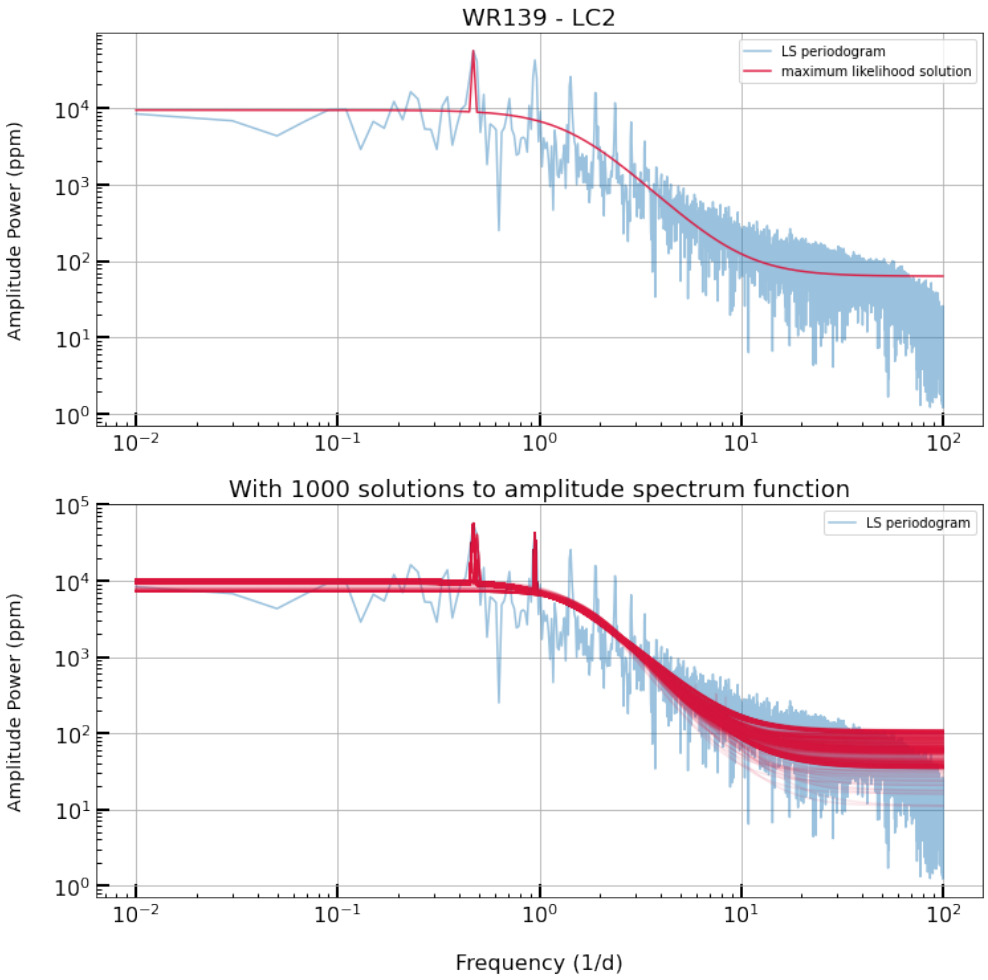

Figure A.24: MCMC amplitude spectrum + Cauchy distribution fits of WR139's Lomb-Scargle periodogram

Appendix B

Wolf-Rayet Stars' Light Curves & Fitting Results

One may find the full set of data and results of all 58 TESS WRs available in my project repository linked here - Y4 Massive Stars Project

Appendix C

Numerical MCMC Fit Parameters of Wolf-Rayet Star's Amplitude Spectrum

Table C.1: Full table of all 58 Wolf-Rayet stars that are observed by the TESS satellite and their associated fit parameters. Results are obtained from fitting their Lomb-Scargle periodograms with the combined amplitude spectrum function + Lorentzian term model stated in Equation 2.1. This table is sorted in the order of their spectral subtypes. Starting from the lowest order of the WC-subtype to WN-subtype single stars, and then towards binary systems with WC-subtype components first and then to WN-subtype components

WR	lc_no	Subtype	α_0 (ppm)	ν_{char} (day^{-1})	γ	C_w (ppm)	ν_0 (day^{-1})	λ
52	0	WC4	111.065	4.208	1.613	8.558	2.8505	0.001947
4	0	WC5	162.042	2.808	1.43	13.041	0.35	0.001616
17	0	WC5	294.44	1	0.889	15.78	3.1211	0.01385
	1		298.696	1	1.012	16.904	74.0375	0.006733
15	0	WC6	191.944	1.44	1.336	12.349	0.1702	0.001496
	1		165.854	1.468	1.273	10.552	0.2716	0.030275
23	0	WC6	145.420	2.630	1.477	7.602	23.125	0.009223
	1		135.004	2.774	1.549	7.874	0.25	0.001311
14	0	WC7	247.933	2.216	1.449	7.189	0.13	0.000906
	1		160.768	3.192	1.574	6.648	1.4702	0.001668

Table C.1: Continued.

WR	lc_no	Subtype	α_0 (ppm)	$\nu_{\rm char}$ (day^{-1})	γ	C_w (ppm)	ν_0 (day^{-1})	λ
90	0	WC7	151.099	2.614	1.315	3.735	10.0472	0.00722
53	0	WC8	288.783	2.764	1.806	13.654	1.2301	0.000604
57	0	WC8	243.568	2.497	1.513	11.911	0.7705	0.000619
59	0	WC9d	441143.934	0.06	1.112	10.292	0.4887	0.003674
103	0	WC9d	4154.569	0.763	1.327	0.1	4.0104	0.000629
3	0	WN3ha	568.49	9.999	1.577	10.435	9.3923	0.002134
46	0	WN3b	46148.913	0.034	0.801	1.639	3.2903	0.000016
	1		6226.767	1.003	0.982	1.005	6.5903	0.000742
6	0	WN4b	5097.674	0.869	20	69.242	1.3301	0.00013
	1		5383.506	0.899	4.378	55.977	0.5301	0.000009
	2		3239.378	0.798	3.061	17	99.9977	9.989019
7	0	WN4b	1000	1.301	1.854	31.726	0.39	0.000039
	1		646.899	1.843	1.912	26.304	0.37	0.000053
18	0	WN4b	380.868	0.724	1.563	18.002	0.11	0.000489
	1		246.238	0.997	1.478	16.662	0.8116	0.001275
	2		491.065	0.998	3.084	31.486	0.47	0.00033
	3		425.255	1	2.523	29.127	0.6101	0.00051
10	0	WN5h	999.988	4.544	3.571	40.868	0.4901	0.000076
24	0	WN6ha	1770.82	1	1.768	9.144	30.6676	0.009516
	1		1924.405	1	1.675	1.006	41.2908	0.039229
	2		1866.449	0.999	1.661	0.541	1.5103	0.000293
43B	0	WN6ha	33085.425	1.051	3.647	397.556	0.5301	0.000002
43C*	0	O3If*/WN6	29061.599	1.089	4.19	287.718	0.5301	0.000001
67	0	WN6o	17796.761	0.42	1.521	73.766	0.15	0.000007
	1		5304.4	1.271	1.868	38.311	0.3701	0.000033
71	0	WN6o	2743.61	1.825	1.421	12.324	0.3901	0.000027

Table C.1: Continued.

WR	lc_no	Subtype	α_0 (ppm)	$\nu_{\rm char}$ ($\rm day^{-1}$)	γ	C_w (ppm)	ν_0 ($\rm day^{-1}$)	λ
75	0	WN6b	869.859	0.692	1.862	19.324	0.1901	0.000041
85	0	WN6h	47.02	0.832	1.34	1.964	4.1445	0.019186
	1		150.113	0.332	1.294	7.79	1.7094	0.005817
78	0	WN7h	1836.177	1.341	3.088	12.091	3.8901	0.001238
87	0	WN7h	1829.506	1.366	3.09	18.411	0.47	0.000178
55	0	WN7o	5148.815	1.284	1.627	20.521	0.13	0.000048
12	0	WN8h	19782.821	0.218	1.974	57.231	1.4101	0.00086
	1		20987.525	0.133	1.224	12.54	0.15	0.000054
16	0	WN8h	10000	0.1	0.949	1	0.05	0.000104
	1		5835.93	0.1	0.809	1	0.31	0.000032
40	0	WN8h	5822.219	0.951	2.05	22.65	1.3107	0.001999
	1		19060.254	0.225	1.296	1.02	1.592	1.31386
	2		5261.176	0.992	2.531	26.822	0.25	0.000007
66	0	WN8(h)	2136.300	1.496	1.511	12.477	6.9307	0.000067
	1		1642.018	1.936	1.670	15.705	6.9307	0.000038
89	0	WN8h	1700.877	1.202	2.846	17.721	0.2102	0.008022
148	0	WN8h	1850.376	1.331	2.414	19.213	0.2901	0.000028
9	0	WC5+O7	298.292	2.566	1.623	9.324	0.6901	0.000286
48	0	WC6+O9.5	2905.549	0.945	2.721	18.915	0.2301	0.000021
	1		2195.538	1.085	2.647	9.585	0.4293	0.006822
86	0	WC7+B0III-I	323.596	9.98	11.746	26.062	6.9907	0.000064
	1		290.884	10	10.996	17.523	6.8507	0.000056
79	0	WC7+O5-8	468.316	1.318	1.342	6.647	6.4907	0.001906
42	0	WC7+O7V	369.832	1.185	1.193	2.75	4.9506	0.002757
93	0	WC7+O7-9	290.211	1.033	1.388	8.631	0.2503	0.002686
50	0	WC7+OB	148.599	1.863	3.82	32.414	0.65	0.000329
11	0	WC8+O7.5III-V	473.977	2.228	2.376	2.857	0.2661	0.082189

Table C.1: Continued.

WR	lc_no	Subtype	α_0 (ppm)	$\nu_{\rm char}$ (day^{-1})	γ	C_w (ppm)	ν_0 (day^{-1})	λ
	1		5727.565	0.359	1.66	26.802	0.05	0.000078
	2		902.704	2.512	2.501	12.595	0.5501	0.000203
	3		1022.075	1.185	1.464	6.207	2.5102	0.000562
70	0	WC9vd+B0I	7659.599	0.228	1.391	0.43	0.43	0.000046
	1		7108.132	0.306	1.492	1.049	0.13	0.00004
69	0	WC9d+OB	4441.259	0.674	1.411	6.387	0.17	0.000016
	1		3697.06	0.919	1.706	7.211	0.2901	0.000116
31	0	WN4o+O8V	1559.925	1.259	1.397	12.831	2.7303	0.000157
21	0	WN5o+O4-6	4354.543	0.344	1.343	10.859	1.61	0.000261
	1		3644.658	0.459	1.252	6.377	0.11	0.000035
141	0	WN5o+O5V-III	1823.219	1.627	1.89	7.884	7.3307	0.000345
139	0	WN5o+O6III-V	12443.232	1.634	3.73	149.571	0.47	0.00001
	1		11224.463	1.619	3.234	160.197	0.47	0.000007
	2		9268.092	1.425	2.576	63.315	0.47	0.000006
97	0	WN5b+O7	550.593	1.563	1.144	6.905	0.3899	0.000404
133	0	WN5o+O9I	1311.362	1.404	2.235	15.447	0.19	0.000165
25*	0	O2.5If*/WN6+O	687.874	2.258	3.62	8.777	1.0697	0.000302
	1		709.141	1.936	3.073	8.816	0.97	0.000031
	2		849.28	1.632	2.328	7.727	0.4699	0.000182
47	0	WN6o+O5V	12604	0.472	1.743	19.56	0.17	0.000019
	1		9828.942	0.452	1.754	36.518	0.17	0.000015
153	0	WN6o/CE+O6I	8985.024	0.649	2.256	50.091	0.31	0.000148
	1		7174.643	0.75	11.965	76.502	1.1501	0.000058
155	0	WN6o+O9II-Ib	11991.807	2.232	6.379	266.336	1.2101	0.000002
43A	0	WN6ha+WN6ha	29254.241	1.117	3.869	376.362	0.5301	0.000002
22	0	WN7h+O9III-V	2269.091	0.828	1.966	20.165	0.6701	0.000193
	1		3192.91	0.814	2.881	13.773	0.31	0.000019

Table C.1: Continued.

WR	lc_no	Subtype	α_0 (ppm)	$\nu_{\rm char}$ ($\rm day^{-1}$)	γ	C_w (ppm)	ν_0 ($\rm day^{-1}$)	λ
	2		2677.546	0.555	1.504	4.056	0.1501	0.000036
98	0	WN8o+WC7	10821.73	0.157	0.928	0.1	94.2108	0.013709
79B	0	WN9ha+O6Iafpe	1776.224	1.556	3.474	22.353	0.3901	0.000142
	1		2133.558	1.192	2.46	10.183	11.0911	0.001368
79A	0	WN9ha+O8Iafpe	2339.043	1.142	2.294	21.861	0.3301	0.000054
	1		2833.051	1.018	5.032	16.658	0.35	0.00008
	2		555.587	0.922	3.418	46.57	0.21	0.000339

Bibliography

R. Blomme, L. Mahy, C. Catala, J. Cuypers, E. Gosset, M. Godart, J. Montalban, P. Ventura, G. Rauw, T. Morel, P. Degroote, C. Aerts, A. Noels, E. Michel, F. Baudin, A. Baglin, M. Auvergne, and R. Samadi. Variability in the CoRoT photometry of three hot O-type stars. HD 46223, HD 46150, and HD 46966. , 533:A4, September 2011. doi: 10.1051/0004-6361/201116949.

Dominic M. Bowman, Siemen Burssens, May G. Pedersen, Cole Johnston, Conny Aerts, Bram Buysschaert, Mathias Michielsen, Andrew Tkachenko, Tamara M. Rogers, Philipp V. F. Edelmann, Rathish P. Ratnasingam, Sergio Simón-Díaz, Norberto Castro, Ehsan Moravveji, Benjamin J. S. Pope, Timothy R. White, and Peter De Cat. Low-frequency gravity waves in blue supergiants revealed by high-precision space photometry. *Nature Astronomy*, 3:760–765, May 2019. doi: 10.1038/s41550-019-0768-1.

P. A. Crowther, Orsola De Marco, and M. J. Barlow. Quantitative classification of WC and WO stars. *Mon. Not. R. Astron. Soc.*, 296(2):367–378, May 1998. doi: 10.1046/j.1365-8711.1998.01360.x.

Paul A. Crowther. Physical Properties of Wolf-Rayet Stars. , 45(1):177–219, September 2007. doi: 10.1146/annurev.astro.45.051806.110615.

Paul A. Crowther and Nolan R. Walborn. Spectral classification of O2-3.5 If*/WN5-7 stars. *Mon. Not. R. Astron. Soc.*, 416(2):1311–1323, September 2011. doi: 10.1111/j.1365-2966.2011.19129.x.

K. Dsilva, T. Shenar, H. Sana, and P. Marchant. A spectroscopic multiplicity survey of Galactic Wolf-Rayet stars. I. The northern WC sequence. , 641:A26, September 2020. doi: 10.1051/0004-6361/202038446.

K. Dsilva, T. Shenar, H. Sana, and P. Marchant. A spectroscopic multiplicity survey of Galactic Wolf-Rayet stars: II. The northern WNE sequence. *arXiv e-prints*, art. arXiv:2204.12518, April 2022.

R. Fahed and A. F. J. Moffat. Colliding winds in five WR+O systems of the Southern hemisphere. *Mon. Not. R. Astron. Soc.*, 424(3):1601–1613, August 2012. doi: 10.1111/j.1365-2966.2012.20494.x.

Daniel Foreman-Mackey, David W. Hogg, Dustin Lang, and Jonathan Goodman. emcee: The MCMC Hammer. , 125(925):306, March 2013. doi: 10.1086/670067.

R. Gamen, E. Gosset, N. I. Morrell, V. S. Niemela, H. Sana, Y. Nazé, G. Rauw, R. H. Barbá, and G. R. Solivella. The first orbital solution for the massive colliding-wind binary HD 93162 (≡ WR 25). In *Revista Mexicana de Astronomia y Astrofisica Conference Series*, volume 33 of *Revista Mexicana de Astronomia y Astrofisica Conference Series*, pages 91–93, August 2008.

W. R. Hamann, G. Gräfener, and A. Liermann. The Galactic WN stars. Spectral analyses with line-blanketed model atmospheres versus stellar evolution models with and without rotation. , 457(3):1015–1031, October 2006. doi: 10.1051/0004-6361:20065052.

W. R. Hamann, G. Gräfener, A. Liermann, R. Hainich, A. A. C. Sander, T. Shenar, V. Ramachandran, H. Todt, and L. M. Oskinova. The Galactic WN stars revisited. Impact of Gaia distances on fundamental stellar parameters. , 625:A57, May 2019. doi: 10.1051/0004-6361/201834850.

S. Hubrig, M. Schöller, A. Cikota, and S. P. Järvinen. The search for magnetic fields in two Wolf-Rayet stars and the discovery of a variable magnetic field in WR 55. *Mon. Not. R. Astron. Soc.*, 499(1):L116–L120, December 2020. doi: 10.1093/mnrasl/slaa170.

Guillaume Lenoir-Craig, Nicole St-Louis, Anthony F. J. Moffat, Herbert Pablo, Gerald Handler, Rainer Kuschnig, Adam Popowicz, Gregg Wade, and Konstanze Zwintz. A Study of the Stochastic Photometric Variability in the Winds of Galactic Wolf-Rayet Stars. *Astrophys. J.*, 925(1):79, January 2022. doi: 10.3847/1538-4357/ac397d.

Lightkurve Collaboration, J. V. d. M. Cardoso, C. Hedges, M. Gully-Santiago, N. Saunders, A. M. Cody, T. Barclay, O. Hall, S. Sagear, E. Turtelboom, J. Zhang, A. Tzanidakis, K. Mighell,

J. Coughlin, K. Bell, Z. Berta-Thompson, P. Williams, J. Dotson, and G. Barentsen. Lightkurve: Kepler and TESS time series analysis in Python. Astrophysics Source Code Library, December 2018.

I. Lundstrom and B. Stenholm. Wolf-Rayet stars in open clusters and associations. , 58:163–192, October 1984.

J. M. Matthews and A. F. J. Moffat. WR 40 : coherence or chaos ? , 283:493–507, March 1994.

A. F. J. Moffat and V. S. Niemela. On the nature of the Wolf-Rayet component in the core of the massive galactic HII region NGC 3603. *Astrophys. J.*, 284:631–636, September 1984. doi: 10.1086/162445.

P. Monderen, C. W. H. De Loore, K. A. van der Hucht, and A. M. van Genderen. Short-timescale light variations of the Wolf-Rayet stars WR 46 and WR86. , 195:179–182, April 1988.

Thierry Morel, Nicole St-Louis, and Sergey V. Marchenko. Optical Spectroscopy of EZ Canis Majoris: Indication for Large-Scale Structures in a Wolf-Rayet Wind. *Astrophys. J.*, 482(1): 470–489, June 1997. doi: 10.1086/304122.

L. M. Oskinova. Evolution of X-ray emission from young massive star clusters. *Mon. Not. R. Astron. Soc.*, 361(2):679–694, August 2005. doi: 10.1111/j.1365-2966.2005.09229.x.

S. J. Paardekooper, P. M. Veen, A. M. van Genderen, and K. A. van der Hucht. On the variability of the visual binary WR86. WC7 with a β-Cephei companion. , 384:1012–1022, March 2002. doi: 10.1051/0004-6361:20020085.

J. C. Pandey, S. B. Pandey, and Subhajeet Karmakar. Phase-resolved XMM-Newton and Swift Observations of WR 25. *Astrophys. J.*, 788(1):84, June 2014. doi: 10.1088/0004-637X/788/1/84.

R. A. Phillipson, P. T. Boyd, and A. P. Smale. The chaotic long-term X-ray variability of 4U 1705-44. *Mon. Not. R. Astron. Soc.*, 477(4):5220–5237, July 2018. doi: 10.1093/mnras/sty970.

R. A. Phillipson, P. T. Boyd, A. P. Smale, and M. S. Vogeley. Complex variability of Kepler AGN revealed by recurrence analysis. *Mon. Not. R. Astron. Soc.*, 497(3):3418–3439, September 2020. doi: 10.1093/mnras/staa2069.

Pragati Pradhan, David P. Huenemoerder, Richard Ignace, A. M. T. Pollock, and Joy S. Nichols. The Colliding Winds of WR 25 in High-resolution X-Rays. *Astrophys. J.*, 915(2):114, July 2021. doi: 10.3847/1538-4357/ac02c4.

G. Rauw, J. M. Vreux, E. Gosset, J. Manfroid, and V. S. Niemela. A new orbital solution for the WNL binary system WR12. In J. M. Vreux, A. Detal, D. Fraipont-Caro, E. Gosset, and G. Rauw, editors, *Liege International Astrophysical Colloquia*, volume 33 of *Liege International Astrophysical Colloquia*, page 303, January 1996.

George R. Ricker, Joshua N. Winn, Roland Vanderspek, David W. Latham, Gáspár. Á. Bakos, Jacob L. Bean, Zachory K. Berta-Thompson, Timothy M. Brown, Lars Buchhave, Nathaniel R. Butler, R. Paul Butler, William J. Chaplin, David Charbonneau, Jørgen Christensen-Dalsgaard, Mark Clampin, Drake Deming, John Doty, Nathan De Lee, Courtney Dressing, E. W. Dunham, Michael Endl, Francois Fressin, Jian Ge, Thomas Henning, Matthew J. Holman, Andrew W. Howard, Shigeru Ida, Jon Jenkins, Garrett Jernigan, John A. Johnson, Lisa Kaltenegger, Nobuyuki Kawai, Hans Kjeldsen, Gregory Laughlin, Alan M. Levine, Douglas Lin, Jack J. Lissauer, Phillip MacQueen, Geoffrey Marcy, P. R. McCullough, Timothy D. Morton, Norio Narita, Martin Paegert, Enric Palle, Francesco Pepe, Joshua Pepper, Andreas Quirrenbach, S. A. Rinehart, Dimitar Sasselov, Bun'ei Sato, Sara Seager, Alessandro Sozzetti, Keivan G. Stassun, Peter Sullivan, Andrew Szentgyorgyi, Guillermo Torres, Stephane Udry, and Joel Villasenor. Transiting Exoplanet Survey Satellite (TESS). In Jr. Oschmann, Jacobus M., Mark Clampin, Giovanni G. Fazio, and Howard A. MacEwen, editors, *Space Telescopes and Instrumentation 2014: Optical, Infrared, and Millimeter Wave*, volume 9143 of *Society of Photo-Optical Instrumentation Engineers (SPIE) Conference Series*, page 914320, August 2014. doi: 10.1117/12.2063489.

C. K. Rosslowe and P. A. Crowther. Spatial distribution of Galactic Wolf-Rayet stars and implications for the global population. *Mon. Not. R. Astron. Soc.*, 447(3):2322–2347, March 2015. doi: 10.1093/mnras/stu2525.

A. Sander, W. R. Hamann, and H. Todt. The Galactic WC stars. Stellar parameters from spectral analyses indicate a new evolutionary sequence. , 540:A144, April 2012. doi: 10.1051/0004-6361/201117830.

A. A. C. Sander, W. R. Hamann, H. Todt, R. Hainich, T. Shenar, V. Ramachandran, and L. M. Oskinova. The Galactic WC and WO stars. The impact of revised distances from Gaia DR2 and their role as massive black hole progenitors. , 621:A92, January 2019. doi: 10.1051/0004-6361/201833712.

O. Schnurr, J. Casoli, A. N. Chené, A. F. J. Moffat, and N. St-Louis. The very massive binary NGC 3603-A1. *Mon. Not. R. Astron. Soc.*, 389(1):L38–L42, September 2008. doi: 10.1111/j.1745-3933.2008.00517.x.

K. Sen, X. T. Xu, N. Langer, I. El Mellah, C. Schürmann, and M. Quast. X-ray emission from BH+O star binaries expected to descend from the observed galactic WR+O binaries. , 652:A138, August 2021. doi: 10.1051/0004-6361/202141214.

Lindsey F. Smith, Michael M. Shara, and Anthony F. J. Moffat. A three-dimensional classification for WN stars. *Mon. Not. R. Astron. Soc.*, 281(1):163–191, July 1996. doi: 10.1093/mnras/281.1.163.

John Southworth and Dominic M. Bowman. High-mass pulsators in eclipsing binaries observed using TESS. *Mon. Not. R. Astron. Soc.*, April 2022. doi: 10.1093/mnras/stac875.

Nicole St-Louis, M. J. Dalton, S. V. Marchenko, A. F. J. Moffat, and A. J. Willis. The IUE MEGA Campaign: Wind Structure and Variability of HD 50896 (WN5). , 452:L57, October 1995. doi: 10.1086/309706.

Ian R. Stevens and Ian D. Howarth. Infrared line-profile variability in Wolf–Rayet binary systems. *Mon. Not. R. Astron. Soc.*, 302(3):549–560, January 1999. doi: 10.1046/j.1365-8711.1999.02151.x.

Daniel Toker, Friedrich T. Sommer, and Mark D'Esposito. A simple method for detecting chaos in nature. *arXiv e-prints*, art. arXiv:1904.00986, March 2019.

Karel A. van der Hucht. The VIIth catalogue of galactic Wolf-Rayet stars. , 45(3):135–232, February 2001. doi: 10.1016/S1387-6473(00)00112-3.

A. M. van Genderen, M. A. W. Verheijen, K. A. van der Hucht, C. W. H. De Loore, H. E. Schwarz, B. P. M. van Esch, H. Greidanus, R. van der Heiden, E. van Kampen, E. Kuulkers, R. S. Le

Poole, R. A. Reijns, F. H. A. Robijn, and L. Spijkstra. (intrinsic) Variations of Wolf-Rayet Stars. In Karel A. van der Hucht and Bambang Hidayat, editors, *Wolf-Rayet Stars and Interrelations with Other Massive Stars in Galaxies*, volume 143, page 129, January 1991.

N. R. Walborn. The O3 stars. , 254:L15–L17, March 1982. doi: 10.1086/183747.

P. M. Williams, K. A. van der Hucht, and G. Rauw. Are WC9 Wolf-Rayet stars in colliding-wind binaries? In G. Rauw, Y. Nazé, R. Blomme, and E. Gosset, editors, *Massive Stars and High-Energy Emission in OB Associations*, pages 65–68, November 2005.